EFFECTS OF CONFINEMENT ON WATER STRUCTURE AND DYNAMICS AND ON PROTON TRANSPORT: A MOLECULAR SIMULATION STUDY

A Thesis

by

PUSSANA HIRUNSIT

Submitted to the Office of Graduate Studies of
Texas A&M University
in partial fulfillment of the requirements for the degree of

MASTER OF SCIENCE

May 2007

Major Subject: Chemical Engineering

EFFECTS OF CONFINEMENT ON WATER STRUCTURE AND DYNAMICS AND ON PROTON TRANSPORT: A MOLECULAR SIMULATION STUDY

A Thesis

by

PUSSANA HIRUNSIT

Submitted to the Office of Graduate Studies of
Texas A&M University
in partial fulfillment of the requirements for the degree of

MASTER OF SCIENCE

Approved by:

Chair of Committee,	Perla B. Balbuena
Committee Members,	James Silas
	Raymond Schaak
Head of Department,	N.K. Anand

May 2007

Major Subject: Chemical Engineering

ABSTRACT

Effects of Confinement on Water Structure and Dynamics and on Proton Transport: A Molecular Simulation Study. (May 2007)

Pussana Hirunsit, B.Eng., King Mongkut's Institute of Technology Ladkrabang, Bangkok, Thailand;

M.Eng., King Mongkut's University of Technology Thonburi, Bangkok, Thailand

Chair of Advisory Committee: Dr. Perla B. Balbuena

Classical molecular dynamics (MD) simulations are performed to study structural and dynamic properties of water confined within graphite surfaces. The surfaces are separated at distances varying between 7 and 14.5 Å and the water density is held constant at 1g/cc. Results at 298 K show the formation of a well-ordered structure constituted by water layers parallel to the graphite surfaces. The water molecules in the layers in contact with the surface have a tendency to orient their dipole parallel to the surface. Such ice-like structures may have different structural and dynamic properties than those of ice. The calculated mean square displacement reveals that the mobilities of the confined water at a separation of 8 Å become similar to that of low-temperature water (213 K) at the same density, although the structures of water are very different. The temperature at which the mobility of water confined at the separation of 7 Å would become similar to that of bulk low-temperature water was found to be 373K. With respect to the dynamics of confined water, a significant blue shift is observed in the intermolecular vibrational modes associated with the O···O···O bending and O···O stretching of molecules linked by hydrogen bonds.

The analysis of the geometry of water clusters confined between two graphite surfaces has been performed using ab initio methods. The ab initio calculations yield two preferential orientations of water molecules which are; 1) one O-H bond points to the surface and the other is parallel; 2) both O-H bonds are parallel to the surface. These orientations agree with those found in our MD simulation results. The calculated energy barriers for proton transfer of the confined H_3O^+-(H_2O) complexes between two graphite

model surfaces suggest that the confinement enhances the proton transfer at the separation 6-14.5 Å. When the confinement is high, at a separation of 4 Å, the barrier energies are extremely large. The confinement does not enhance proton transfer when the H_3O^+-(H_2O) complexes are located further from the surfaces by more than 8 Å. As a result, the barrier energies start to increase at the separation of 20 Å.

To my mother, my father and my lovely sister

ACKNOWLEDGEMENTS

I would like to acknowledge the help of many people in this research effort. I am especially grateful to Prof. Perla B. Balbuena who gave me the appreciable suggestions, counsel, and encouragement throughout the period of this work. My gratitude is also extended to the committee members, Dr. James Silas and Dr. Raymond Schaak, in making useful and helpful comments.

Furthermore, I extend my gratitude to the National Nanotechnology Center in Bangkok Thailand for providing me with support in the form of a scholarship. Special thanks also goes to Sergio Calvo, Eduardo Lamas, Gu Zhihui, and Jin Zhao, who are PhD students in Dr. Balbuena's group. They provided technical assistance with the programs and attempted to answer all of my many questions. Also, I would like to thank Mr. Robert Rose for his editorial assistance and attentive care when I was sick. Finally, I wish especially to thank my mother, my father and my sister for their constant love and endless support from my home, so far away, in Bangkok.

TABLE OF CONTENTS

CHAPTER Page

LIST OF FIGURES

FIGURE Page

LIST OF TABLES

CHAPTER I

INTRODUCTION

1.1. Water confined in carbon nanostructures

The behavior of water confined in carbon nanostructures has many interesting implications in chemical, biological, and electrochemical fields. Several related applications have already been explored in the chemical, oil and gas, food, and pharmaceutical industries [1]. Our fundamental understanding of the behavior of confined water has been enriched by the study of water adsorption isotherms [2], density distribution and water clustering growth [3] in carbon nanopores. Such behavior is influenced by water interactions with hydrophobic species in nanoenvironments such as those arising in water channels present in living organisms [3, 4]. Furthermore, water in carbon nanotubes has been actively studied because its presence could alter the physical, chemical, and electronic properties of the nanotubes [5, 6], which are sought as potential materials for electronics and biomedical devices.

In similarity to other systems in the nano regime, the structure and properties of water confined in nanoscale spaces may be very different from those of the bulk. X-ray diffraction experiments by Iiyama et al [7, 8] to determine the structure of a water molecular assembly in a hydrophobic nanospace with characteristic widths in the range of 1.13 nm between 148K and 303K, illustrated that confined water in carbon nanotubes shows solid-like structure. These authors showed that X-ray diffraction patterns of water adsorbed in slit-shaped carbon pores contain sharp peaks, contrasted with no sharp peaks in the spectra of bulk liquid water. These sharp peaks suggest that the water molecules have an ordered, ice-like structure, which is plausible along the horizontal direction of the slit pore [7]. Experimental X-ray diffraction results also showed that the structure of water molecules confined in the same hydrophobic environment with pore widths of 0.75nm at 303 K is more ordered compared with that of 1.13nm without phase transition detected as a function of the pore size [8].

This thesis follows the style of Physical Review E.

In addition, molecular simulations of the behavior of water encapsulated in carbon nanotubes were reported by Koga et al [9]. The simulations were performed using carbon nanotube diameters ranging from 1.1nm to 1.4nm and applied axial pressures of 50 to 500 MPa. The results showed the existence of a new ice phase (Figure 1.1), unlike any of the known bulk ice structures, which displayed a first-order transition to hexagonal and heptagonal ice nanotubes and a continuous phase transformation into solid-like square or pentagonal ice nanotubes [9]. Similarly, Striolo et al [5] performed simulations of water in single-walled carbon nanotubes and observed layered ice-like structures.

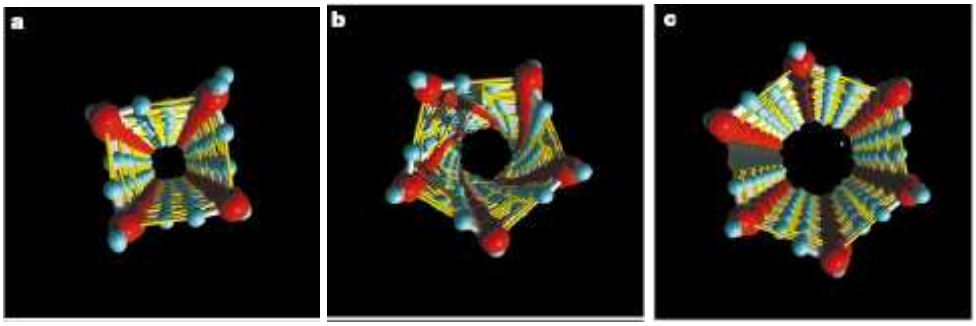

Figure 1.1. Snapshots of quenched molecular coordinates. a, Square ice nanotubes in (14,14) SWCNs; b, pentagonal nanotubes in (15,15) SWCNs; c, hexagonal ice nanotubes in (16,16) SWCNs; The ice nanotubes were formed on cooling under an axial pressure of 50 MPa in molecular dynamics simulations [9].

One of the potential applications of the ice-type structures formed due to water confinement in hydrophobic structures is the use of these structures as proton-conductor media. Proton transport in aqueous solutions is fundamental to many biological and technological processes [10]. For technological processes, since the early days of the industrial revolution, there have always been devices which depend on proton transport. Most conventional batteries rely on the proton conductivity of the corresponding

aqueous electrolyte and at least some mixed conductivity (protonic and electronic) in the active electrode masses [10], as do many conventional gas sensors operating around room temperature. Even large-scale fuel cells with a power output in the MW range benefit from the high proton conductivity of phosphoric acid. Besides these traditional applications, the progressive availability of solid proton-conducting materials stimulates the utilization of proton conduction in a variety of devices for energy conversion, chemical sensing, the production of chemicals [10].

1.2. Proton transport in water confined in nanostructure systems

Dellago et al [11] have studied a system of proton transport along a single file of oriented water with hydrogen-bonding defects through water-filled carbon nanotubes using molecular dynamics (MD) simulations. They reported that charges and defects interact strongly, and such interaction causes them to diffuse together. The diffusion coefficient of the defect is of the order of 3-4 $Å^2$/ps, much lower compared with the proton diffusion constant of 17 $Å^2$/ps, when uncoupled from the motion of the defect. Moreover, Mann et al [12] investigated proton transport along a one-dimensional water wire encapsulated inside (6,6) single-walled carbon nanotubes. Their simulation results suggested that a proton in presence of neutral water tends to stay inside the carbon nanotubes rather than to achieve complete conduction through the nanotube interior. Instead, a proton rapidly diffuses from end to end under the presence of a small electric field applied along the carbon nanotube axis. These proton transport systems are believed to mediate proton conduction following a Grotthuss mechanism [13] involving proton hopping rather than molecular diffusion. The Grotthuss mechanism is that proton tunnel from one water molecule to the next via hydrogen bonding as shown in Figure 1.2.

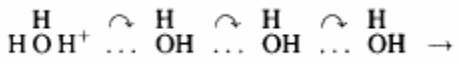

Figure 1.2. Grotthuss mechanism of proton transport [13].

1.3. Molecular dynamics simulation

Molecular dynamics is a powerful method for exploring the structure of solids, liquids and gases. The idea is a simple one. The molecular dynamics simulation method is based on Newton's second law or the equation of motion, F = ma, where *F* is the force exerted on a particle, *m* is its mass and *a* is its acceleration. From knowledge of the forces on each atom, it is possible to determine the acceleration of each atom in the system. Integration of the equations of motion then yields a trajectory that describes the positions, velocities and accelerations of the particles as they vary with time. When enough information on the motion of the individual atoms has been gathered, it is possible to condense it all using the methods of statistical mechanics to deduce the bulk properties of the material. Therefore, from the trajectory, the average values of properties can be determined. The method is deterministic; once the positions and velocities of each atom are known, the state of the system can be predicted at any time in the future or the past. Properties that can be determined include the structure, thermodynamics (e.g. enthalpy, temperature, pressure) and transport properties (e.g. thermal conductivity, viscosity, diffusion). Molecular dynamics simulations can be time consuming and computationally expensive. However, computers are getting faster and cheaper. In addition molecular dynamics can be used to investigate the detailed atomistic mechanisms underlying these properties and compare them with theory. It is a valuable bridge between experiment and theory.

1.4. Ab initio methods

Ab initio molecular orbital theory enables the calculation of molecular parameters such as geometry and energy of molecules or molecular complexes, by solving the Schrödinger equation, without requiring any experimental data or assumptions from the system under study.

Ab initio method is defined by two components, a theoretical method and a basis set. The theoretical method usually specifies the level of electron correlation considered. In general, the greater the level of electron correlation considered, the more accurate the

results; however it requires the use of computer resources (RAM, hard disk space and computation time). The basis set gives a mathematical description of the orbitals used to calculate the total electronic wave function of the system. Again, the larger the basis set, the more accurate the results, but the greater the use of computer resources.

1.5. Motivation and objectives

It is well established that water structures formed within the confinement of hydrophobic structures are a plausible effective proton-conductor medium, and hence this is worthy of further study. This work focused on characterizing the structure and dynamics of water at room temperature and a density of 1 g/cm^3 within graphite walls of different separations. This research seeks to establish differences between the structural and dynamic properties of confined water and those of low-temperature water at the same density using classical molecular dynamic simulations. The results could be useful in describing the environment in which a proton would move under these conditions.

However, the classical molecular dynamic simulations in the preliminary study did not include H…C interactions in the force field. Also, it has been reported that water orients on a benzene molecule with one of the H atoms orienting to the surface [14, 15]. Nevertheless, the effect of additional molecules on such orientation is not known. In order to investigate this point, the analysis of the geometry of water clusters using ab initio calculations has been done. Once such water distribution was established via ab initio calculations, the investigation of the proton mobility for the system of confined water within the graphite surfaces using the same method has been done. Note that classical molecular dynamics cannot provide an accurate description of proton transport due to the quantum nature of the proton, which cannot be well described using effective force fields.

The objectives of this study focusing on understanding:

1. The structure and dynamics of water at room temperature and a fixed density within parallel graphite walls at various separations, using classical molecular dynamic simulations, in comparison to bulk low-temperature water of the same density.

2. The geometry of water clusters confined within model graphite surfaces using ab initio calculations.
3. The barrier for proton transfer from a hydronium ion in a confined environment using ab initio calculations.

CHAPTER II

METHODOLOGY

2.1. Molecular dynamics simulation procedures

2.1.1. Force fields

The simple point charge-extended (SCP/E) model is used for water [16]. The water model is represented as a sphere with an oxygen atom located in its center, and the hydrogen atoms 1.0 Å away, with an H-O-H angle of 109.5 ^{o}. The charge on the oxygen site is -0.8476*e* and 0.4238*e* on each of the hydrogen sites. Van der Waals interactions between atoms are described by a 12-6 Lennard-Jones (LJ) potential and the Ewald Sum technique is applied to account for the truncation of the long range electrostatic forces [17]. The LJ potential function is

$$U(r) = 4\varepsilon_{ij}\left[\left(\frac{\sigma_{ij}}{r_{ij}}\right)^{12} - \left(\frac{\sigma_{ij}}{r_{ij}}\right)^{6}\right] \tag{2.1}$$

ε_{ij} and σ_{ij} are the LJ potential parameters that characterize the size and strength of the potential, and r_{ij} is the distance between the centers of mass of the pair atoms. The model parameters of the like interaction are given in Table 2.1, whereas those for the unlike interaction are calculated by the Lorentz-Berthelot combining rules;

$$\sigma_{ij} = \frac{\sigma_{ii} + \sigma_{jj}}{2}$$

$$\varepsilon_{ij} = \sqrt{\varepsilon_{ii}\varepsilon_{jj}} \tag{2.2}$$

Table 2.1. LJ potential parameters for carbon-carbon (in graphite) and oxygen-oxygen (in water) interactions.

Pair interaction	ε_{ij} (kcal/mole)	σ_{ij} (Å)
O_{water} - O_{water} [16]	0.1553	3.166
C - C [18]	0.0553	3.400

2.1.2. Building the system

To analyze the confinement effect of water between walls of a hydrophobic material, a graphite slab made of two layers was incorporated into the unit cell to simulate a slit pore containing water at 1 g/cc and 298 K. The slit pore model is constructed such that graphite-like crystallites are semi-infinite and composed of two-layer graphite slabs aligned parallel to one another and separated by a distance H (Figure 2.1), which has been given values of 14.5, 11, 8, and 7 Å. The dimensions of the graphite slab are 17 x 19.68 Å. The volume of the system was calculated by excluding the volume occupied by the graphite slabs (Figure 2.1). Because of the periodic boundary conditions imposed on the system in the three spatial directions, water in the box is confined between the graphite slab in the bottom of the unit cell and the graphite slab located in the bottom of the next periodic cell. MD simulations are performed in the canonical NVT ensemble with the Evans thermostat [17], using the DL-POLY program [19]. The equilibration time is set to be 300 ps and the time step 0.001 ps, with production times of 500 ps. After the system reaches equilibrium, the structural and dynamic properties are analyzed.

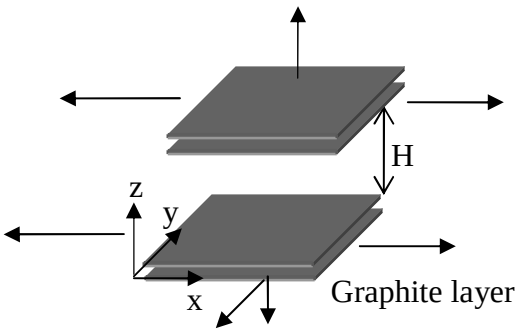

Figure 2.1. Schematic of the slit pore model.

2.1.3. Analysis of the simulation data

2.1.3.1. Radial distribution function

The radial distribution function (RDF) describes how, on average, the atoms in a system are radially packed around each other. The structure is analyzed using the pair radial distribution function, $g_{XY}(r)$, given by the ratio $\rho_{XY}(r)/\rho_{bulk}$, where $\rho_{XY}(r)$ is the local density of atoms *Y* located at position r from the center of atom *X*, and ρ_{bulk} is the bulk density of atoms *Y*, and *r* is the radial distance measured in concentric spherical shells from the center of atom *X*.

2.1.3.2. Mean square displacement

The molecular diffusion is analyzed through the time evolution of the mean square displacement (MSD), a measure of the average distance that a molecule travels, which is defined as:

$$MSD(t) = \left\langle \left| r_i(t) - r_i(t_0) \right|^2 \right\rangle \tag{2.3}$$

with the quantity in brackets averaged over many different initial times t_0. Due to the geometry of this system, The MSD of confined water molecules is computed in the (x-y) direction, according to:

$$MSD(t) = \left\langle \left| x_i(t) - x_i(t_0) \right|^2 + \left| y_i(t) - y_i(t_0) \right|^2 \right\rangle \tag{2.4}$$

The limiting slope of the MSD(t), considered for time intervals sufficiently long for it to be in the linear regime, is related to the self-diffusion constant D:

$$D = \frac{1}{\delta} \lim_{t \to \infty} \frac{d\left\langle \left| r_i(t) - r_i(t_0) \right|^2 \right\rangle}{dt} \tag{2.5}$$

where δ depends on the space dimensionality (6 for three dimensions, 4 for two dimensions).

2.1.3.3. Velocity auto-correlation function

Further insights into the dynamics of the system are obtained by analysis of the normalized velocity autocorrelation function (vacf) [17]. The vacf is a prime example of

a time dependent correlation function, and is important because it reveals the underlying nature of the dynamical processes operating in a molecular system. It is defined as follows:

$$C_v(t) = \frac{\langle v_i(t) v_i(t_0) \rangle}{\langle v_i(t_0)^2 \rangle} \tag{2.6}$$

where $v_i(t)$ is the velocity of O atoms in molecule i at time t, and the brackets indicate ensemble average over many initial times t_0. In this work, the vacf of water molecules is also computed in the lateral (x-y) direction.

As well as revealing the dynamical processes in a system, the vacf has another interesting property. It may be Fourier transformed to project out the underlying frequencies of the molecular processes. This is closely related to the infra-red spectrum of the system, which is also concerned with vibration on the molecular scale.

2.2. Ab initio molecular simulation procedures

2.2.1. Simulation procedures for water clusters confined within model graphite sheets

A sequence of water clusters of increasing size $(H_2O)_n$ n =1-4 confined between two parallel model graphite sheets have been investigated using ab initio calculations. Each of the graphite sheets were initially modeled as a benzene ring, and then by a naphthalene ($C_{10}H_8$) molecule. Since many studies [14, 15, 20] have confirmed that the geometry of the complex is less sensitive to the theoretical level applied, and reasonable results are obtained already at the MP2 level of ab initio molecular simulations, this method has been applied. The MP2 calculations were carried out along with the basis set 6-31G(d) to evaluate geometry structures of the water clusters and proton transport in the system. All the ab initio calculations were done with the GAUSSIAN 03 [21] program.

Initially, the optimizations of the geometry of water clusters $(H_2O)_n$ n = 1-4 on a model graphite sheet were done, in order to verify if the given results were reasonable by comparing them with those reported by others [14, 15, 22] who applied a higher level of theory, and with the available experimental data [23]. Furthermore, these results were

used to investigate how the geometry of water clusters change under confinement within two model graphite sheets.

The geometry of water clusters $(H_2O)_n$ n = 1-4 in the confined system were optimized under the restriction that the x-y coordinates of the benzene rings were frozen, but the z-coordinate that reflects the separation between benzene planes and water clusters were allowed to change. The studied system was built initially with 2 benzene rings, and subsequently with 4 benzene rings, as model graphite surfaces encapsulating water molecules as shown in Figure 2.2.

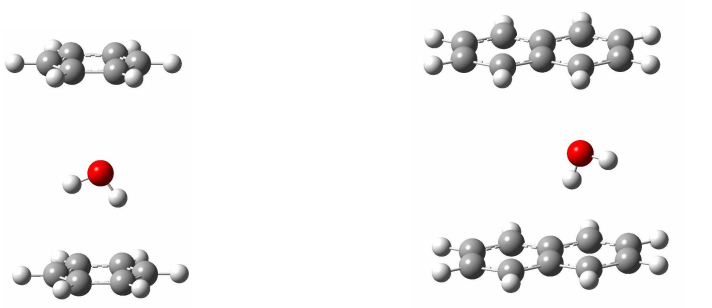

(a) (b)

Figure 2.2. Schematic of the confined water system for ab initio MP2 calculations. (a) water confined between 2 benzene rings. (b) water confined between 4 benzene rings.

2.2.2. Simulation procedures to study proton transfer within the confined system

The hydronium ion (H_3O^+) is optimized using density functional theory (DFT) calculations with the B3PW91 functional and the 6-311++g(d,p) basis set. Its optimized structure shows a flattened trigonal pyramid structure (O-H bond length 0.98 Å, H-O-H angle 113.33^o). The H_3O^+ was located in the vicinity of water clusters $(H_2O)_n$ n = 1-4 confined between the model graphite sheets as shown in Figure 2.3. Then, the system was optimized to determine where the hydrated proton locates in the confined geometry according to the MP2/6-31G(d) method/basis set.

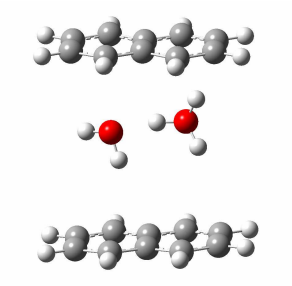

Figure 2.3. Schematic of a hydronium ion-water confined system.

According to the Grotthuss mechanism of proton transport [13], the proton propagates along the O-H···O hydrogen bond direction of the H_3O^+-$(H_2O)_n$ complexes. Tao Li et al [24] have studied the potential energy surface barrier (Figure 2.4(b)) for proton transfer between two water molecules as a function of the OH distance (R_2) and parametric in the O-O distance (R_1) as defined in Figure 2.4(a). Li et al [24] observed that with decreasing R_1 distance between the two oxygen atoms, the activation barrier for proton transfer decreases sharply, and at a certain small R_1 value, the transfer is barrier-free.

In this work, we analyze how the barrier energy for proton transfer from a hydronium ion changes in a confined environment, as the proton propagates along the O-H···O hydrogen bond direction of the H_3O^+-$(H_2O)_n$ complexes according to the Grotthuss mechanism. At a fixed R_1 distance, the R_2 distances were scanned using the optimized geometry obtained from H_3O^+-(H_2O) confined between the two graphite sheets. Then, the analysis was repeated for different values of the R_1 distance.

The results of the calculated potential energy surfaces for the confined systems provided an estimate of the barrier for proton transfer for water in confined geometries. Moreover, the separation distances between walls were varied to study if there is any influence of the proximity of the walls on the barrier.

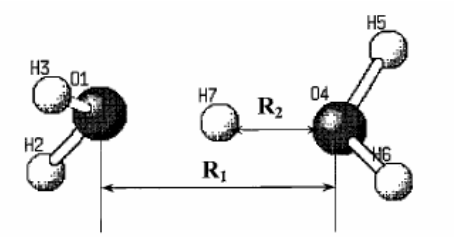

(a)

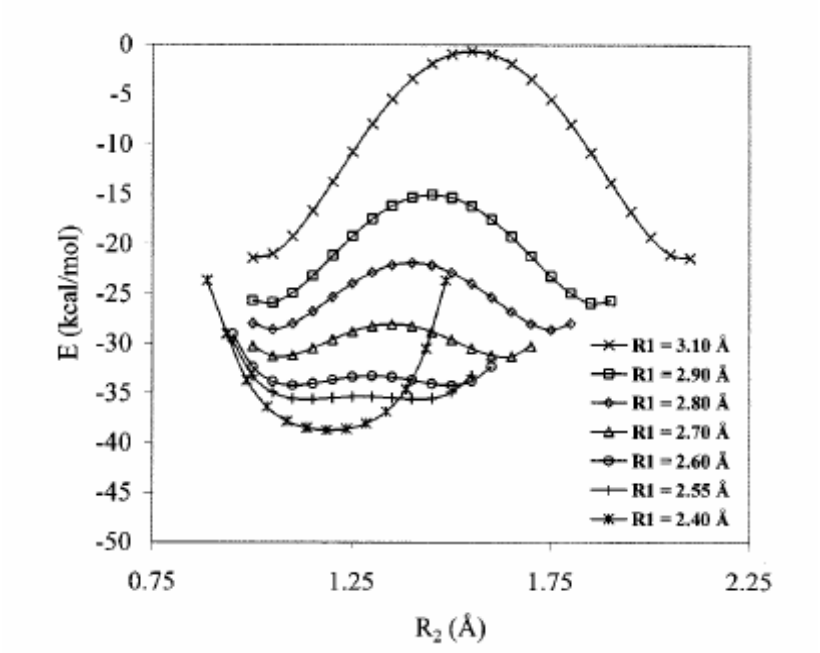

(b)

Figure 2.4. (a) Coordinates used for a potential energy surface scan [24]. (b) Potential energy surface taken from Ref. 24 for proton transfer between two water molecules as a function of the OH distance (R_2) and parametric in the O-O distance (R_1), as defined in (a). The energy E is the energy difference between the energy of the H^+-$(H_2O^+)_n$ complex and the energies of the isolated monomers (H_3O^+ and H_2O) [24].

CHAPTER III

RESULTS AND DISCUSSION

3.1. Molecular dynamics simulation of water confined within graphite surfaces

MD simulations of bulk SPC/E water were performed at 1 g/cm^3 and at 213, 298, and 375K. For the SPC/E model, the melting point of ice has been reported at 213 K [25]. The self-diffusion coefficients calculated according to equation (2.5), are 7.33×10^{-11}, 1.26×10^{-9}, 2.50×10^{-9} and 7.45×10^{-9} m^2/sec at 213K, 270K, 298K and 375K, respectively. The calculated value at 298K is fairly consistent with experimental water self-diffusion coefficient of 2.30×10^{-9} m^2/sec at 298.2K [26]. SPC/E diffusion coefficients of low-temperature water have been reported in a wide range of temperatures and densities [27]. The calculated SPC/E diffusion coefficient at 210K and at a density of 1 g/cm^3 is 1.03x 10^{-11} m^2/sec [28], which is in fair agreement with the calculated value from this work at 213K. Simulations of hexagonal ice for the SPC/E model were reported by Trout et al [29] who determined a slope of 1.4x10^{-12} m^2/sec for the MSD curve at 200K. Using equation (2.5) this slope yields a diffusion coefficient of 2.3 x10^{-13} m^2/sec, one order of magnitude smaller with respect to that of low-temperature water at the same density (0.917 g/cm^3) and 210 K [28]. However, Trout et al's simulation was designed to measure the diffusion of interstitial water, and therefore, their final result is reported as the product of the calculated coefficient from equation (2.5) times the concentration of interstitial water molecules, yielding a much lower value of 1.3 x 10^{-18} m^2/sec at 200K and density of 0.917 g/cm^3. This last value is in good agreement with experiments by Goto et al [30], where an interstitial mechanism is proposed for the self-diffusion of water in ice . In this work, the dynamics of confined water were compared with those of low-temperature water at the same density. For reference, this discussion also include the result of the MSD from ice (with density 0.917 g/cm^3) as obtained by Trout et al [29].

Figure 3.1 shows the density profile of confined water at 1 g/cc in a direction Z perpendicular to the graphite walls, which corresponds to the number density of oxygen atoms belonging to water molecules found in planes parallel to the graphite surfaces (Z-

density). It is observed that there are four layers of water molecules distributed in the slit pore for H = 14.5 Å, three layers for H = 11 Å, and two layers at H = 8 Å and H = 7 Å.

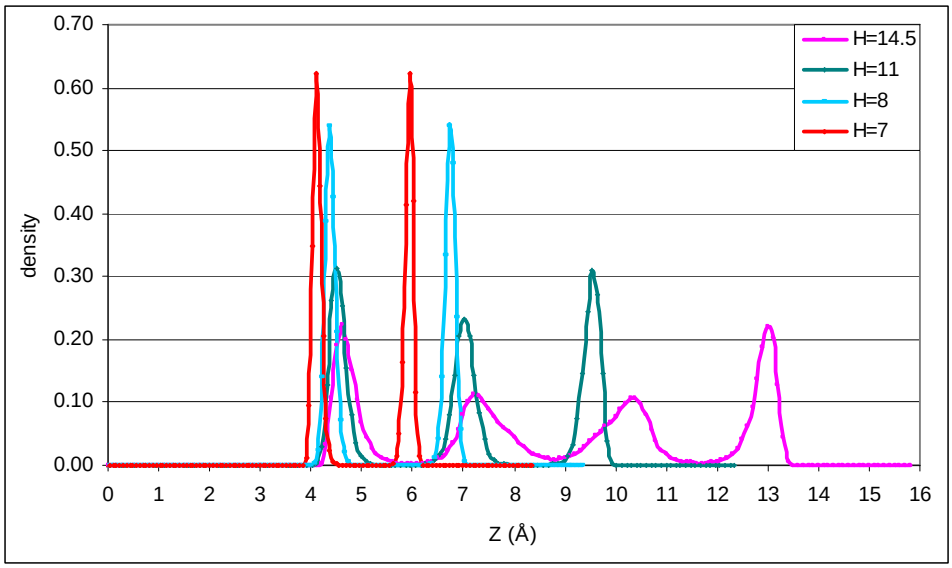

Figure 3.1. Z-density of oxygen atoms in water molecules at different separations H (in Å) between the walls of a slit pore, at 298 K. The walls are located at the left and right of the highest density peaks observed in the graph for each value of H. The separation between the first peak and the wall is approximately 2.7 Å for H = 7, 3 Å for H = 8, 3.1 Å for H = 11, and approximately 3.2 Å for H = 14.5 Å.

Each of the profiles for a given value of H is symmetric; the highest peaks are always in contact with the walls, and their widths become sharper, solid-like, as H decreases (Figure 3.1). These observations are in agreement with other reports [2, 5, 6, 8, 9, 31].

The water structure illustrated in the snapshots shown in Figure 3.2, agrees with the experimental results carried out by Iiyama et al [7, 8] who observed long range well-ordered water molecules in the horizontal direction of a slit pore at room temperature.

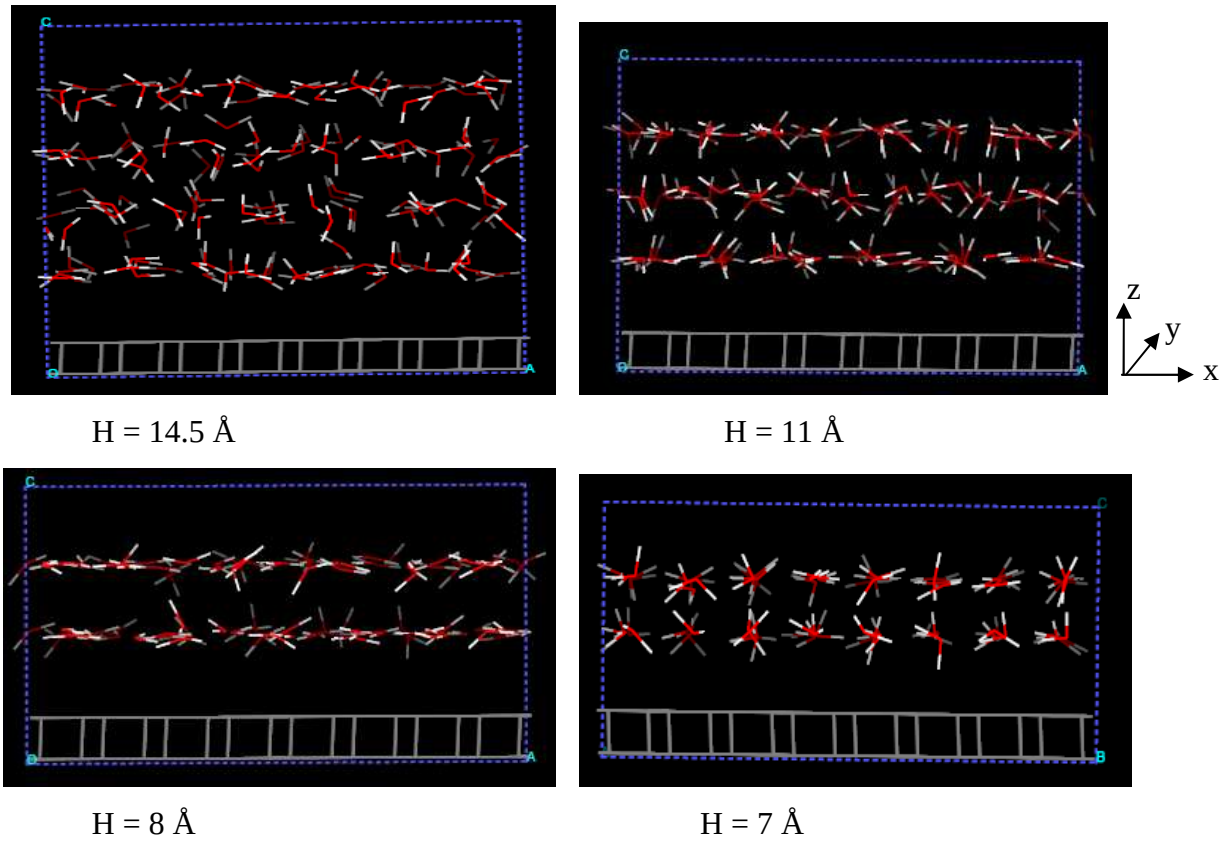

Figure 3.2. Snapshots of water molecules confined between graphite slabs where H is the separation between walls, at 298 K.

Most of the water molecules located in the layers next to the walls orient with both of the hydrogen atoms located nearly in the same plane with its corresponding oxygen atom (Figure 3.2). Analysis of the density profiles shown in Figure 3.3 indicates that the distribution of hydrogen atoms in the water layers in contact with the surfaces are broader, therefore there are a number of hydrogen atoms located closer to the graphite surface than the corresponding oxygen atoms. On the contrary, there is a group of hydrogen atoms in the intermediate layers which are located farther from the graphite surfaces than their corresponding oxygen atoms. Similar results regarding the presence of H atoms closer to the walls were reported by other authors [32, 33]. Pertsin and Grunze [33] incorporated H···C parameters in their Lennard Jones potential, to match

results of ab initio calculations indicating that the most stable configuration of a water molecule in contact with graphite is that with a hydrogen atom pointing to the surface. Note however that such ab initio calculations result from the interaction of a single water molecule with a surface, which obviously will be greatly affected by the presence of other water molecules interacting strongly between them via hydrogen bonds.

In these simulations, even though the results agree with finding some H atoms closer to the walls, the interaction potential employed does not include H…C interactions. Note that Figure 3.3 shows that although hydrogen atoms in the layer adjacent to the graphite surface are found in positions closer than those of oxygen atoms, the peaks of oxygen and hydrogen atoms are nearly at the same position.

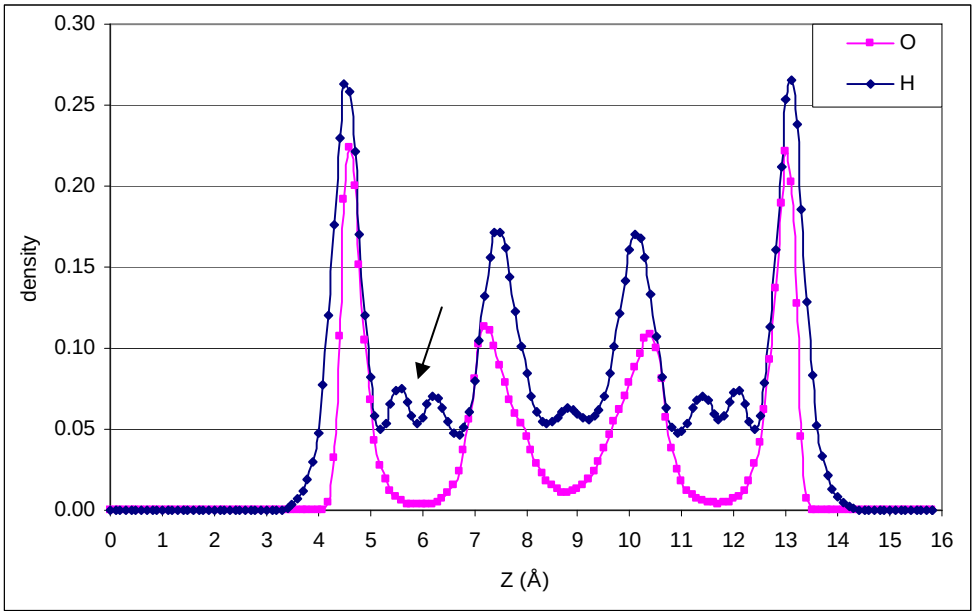

Figure 3.3. Z-density profiles of oxygen and hydrogen atoms of water molecules in a slit pore at H = 14.5 Å and 298 K. The walls are located at the left and right of the highest density peaks. The separation between the first peak and the wall is approximately 3.2 Å. Note that in the layers close to the wall, there is a small number of hydrogen atoms (represented by the small peak indicated by an arrow) located out of the plane where that water molecule resides. In the inner layers, a few H atoms are below the planes of their respective water molecules and most of H atoms of those water molecules in the layer are above those planes, as shown by the peak of H atoms located shifted towards the center of the pore with respect to the peak of oxygen atoms in that layer. These results suggest that water molecules in contact with the carbon surface have a higher tendency to orient their dipole parallel to the surface.

Thus, these results reveal that there are two preferential orientations of water molecules in the layer close to the surfaces: the first one has both OH bonds parallel to the surface, and the second one has one OH pointing to the surface and the other parallel. Also, the first orientation is less frequently found in water molecules located in layers away from the graphite surface (i.e., in the center of the pore) where the interaction forces between the carbon surface and the water molecules become weakened as observed in Figure 3.3. Furthermore, the water molecules at the center of the pore prefer to orient maximizing the number of hydrogen bonds.

The confined water properties can be further investigated by analysis of a dynamic property, the MSD of oxygen atoms shown in Figure 3.4. The MSD of H = 14.5 Å is considerably higher than H = 8 Å. The water self-diffusion coefficient, given by equation 2.5, increases when H increases, in agreement with previous reports [34]. Interestingly, the MSD of low-temperature water at 213 K is very similar to the case of confined water at H =8 Å. Note that at higher values of H (H = 14.5 Å, Figure 3.4), the average mobility is much higher than that of low-temperature water, even though the layers close to the walls still maintain the frozen structure as shown in Figure 3.2. On the other hand at the smallest separation, H = 7 Å, the average diffusion coefficient is much lower than low-temperature water at the same density of 1 g/cc, being of the same order of magnitude as that reported by Trout et al [29] from simulations of SPC/E hexagonal ice at 0.917 g/cm^3 and 200K.

These results imply that the mobility of water molecules significantly decreases under extreme confinement at H $\leq$ 8 Å, in contrast to the persistent mobility reported by Leng and Cummings [34] for water between moving mica sheets, where the smallest size is 9.2 Å. Such difference in dynamic behavior may be attributed not only to the different nature of the surfaces (hydrophilic vs. hydrophobic) but also to the presence of an external field given by the shear force. Similarly, Kalra et al [31] observed that a water layer confined between carbon nanotube membranes which are separated by the distance approximately 3 Å still remains fluid while flowing through the membranes under an osmotic pressure gradient, and Vaiteheeswaran et al [35] who analyzed the

effect of an applied electric field on the structure of confined water between graphite walls, found that the density of the water film decreases and evaporation takes place.

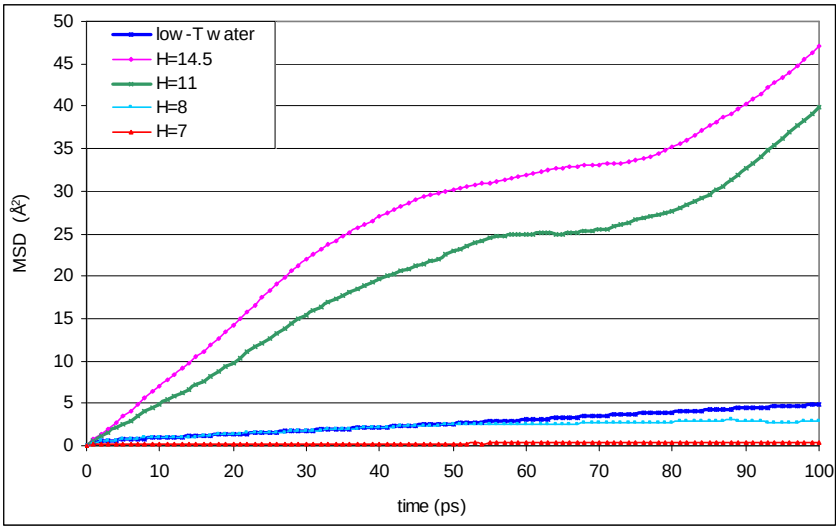

Figure 3.4. MSD of bulk low-temperature water (213 K) and confined water at different separations H (in Å) between the graphite layers at 298 K. The MSD of water in the H = 8 Å pore at 298 K is very similar to that of bulk low-temperature water (213 K). For reference, the diffusion coefficient calculated from the MSD for H = 7 Å, is 7 x 10^{-13} m^2/sec, of the same order of magnitude as that reported by Trout et al for hexagonal ice (2.3 x 10^{-13} m^2/sec) [29].

Definitely these external fields (in addition to the surface external potential exerted on the confined fluid) induce other effects in the system, but they cannot be directly compared with the results from this work.

The structures shown by the radial distribution functions for low-temperature and confined water are substantially different (Figure 3.5). For example, the $g_{oo}(r)$ for H = 14.5 and 11 Å have much broader first peaks which clearly show the departure from the ice tetrahedral structure. Starr et al [28] proposed that the structure of low-temperature

low-density water was similar to low-density amorphous (LDA) solid-water, consisting of an open tetrahedral network, whereas with increasing density the structure becomes closer to that of high-density amorphous (HDA) solid water, similar to water under pressure. This work utilizes a density of 1 g/cm^3, which is closer to the LDA system. Integration of the $g_{oo}(r)$ until the minimum after the first peak yields 14 water molecules, whereas a value of 4 is obtained in the case of low-temperature water corresponding to four waters in tetrahedral structure, each one participating in four H-bonds. Thus, the broad first peak in confined water includes molecules in a given layer plus those in the first neighbor layer (s). For H = 8 Å, the calculated number of water molecules in the first shell reduces to 10.

Figure 3.6 illustrates that the water molecules distribute approximately one per ring; i.e., each molecule has 6 nearest neighbors in the same layer. The measured separation between layers for H = 8 Å is 3.8 Å, which is the distance of the minimum after the first peak (Figure 3.5, top), therefore, the other four water molecules found in the first coordination shell must come from molecules temporarily residing in the interlayer, as illustrated by the snapshot in Figure 3.2. This structure (see right image) resembles the "low-energy" amorphous phase described by Koga and Tanaka [36] (their Figure 5b) which may exist at low temperature and strong confinements (3 <H < 6 Å) according to the phase diagram reported by these authors.

Integration of the first peak of the $g_{OH}(r)$ for low-temperature water yields two H atoms that are forming H-bonds with an oxygen atom; these are two of the four H-bonds in which the water molecule participates, the other two bonds result from the involvement of each of its H atoms with the O atoms of another two molecules. In confined water, integration of the first peak of the $g_{OH}(r)$ also yields two H atoms. However, the tetrahedral arrangement is broken. The position of the first peak in the $g_{OH}(r)$ shifts left as the confinement increases (1.78 Å in low-temperature water, 1.73 Å for H = 14.5 and 11 Å, 1.71 for H = 8 and 1.69 Å for H = 7 Å). The shorter the O···H distance in the H-bond, the strongest and more linear the H-bond structure (the OHO angle will tend to 180^o). The layered structure and the distribution shown in Figure 3.6

are responsible for the broadening of the second peak in the $g_{OH}(r)$, and induces large changes in the $g_{HH}(r)$ (Figure 3.5).

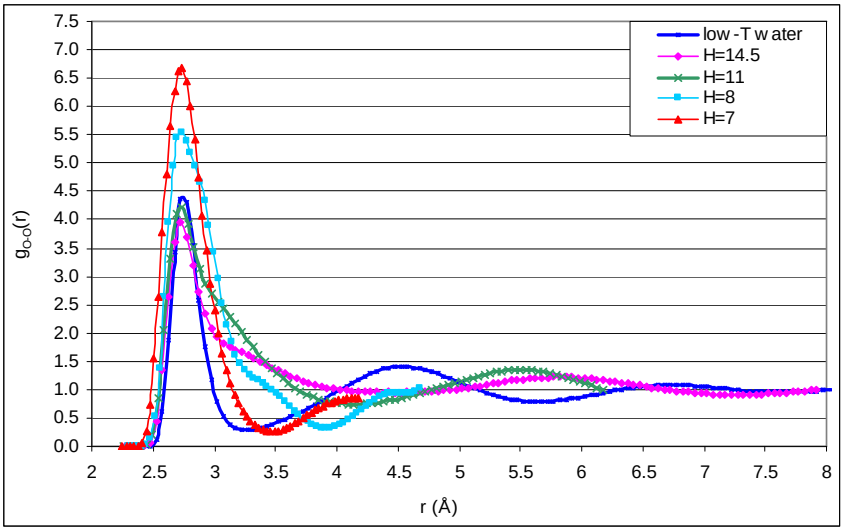

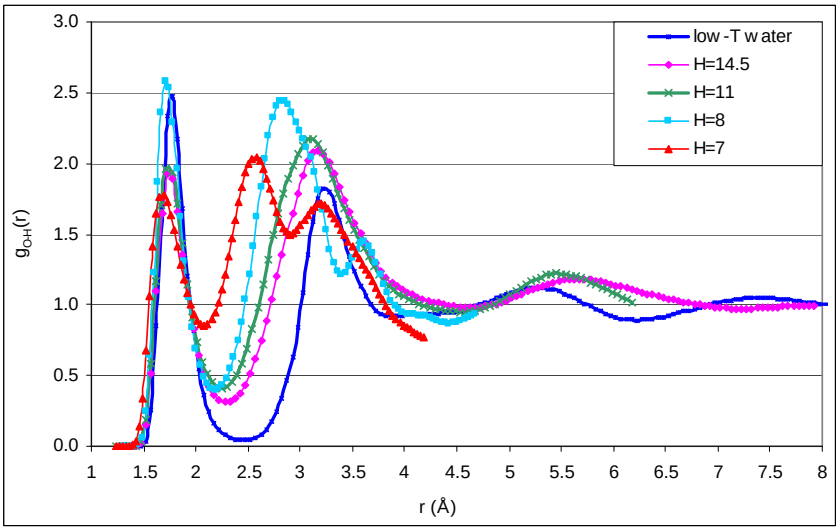

Figure 3.5. $g_{O\text{-}O}(r)$, $g_{O\text{-}H}(r)$, and $g_{H\text{-}H}(r)$ of low-temperature (213 K) and confined water (298K) at various separations H (in Å) between the graphite walls.

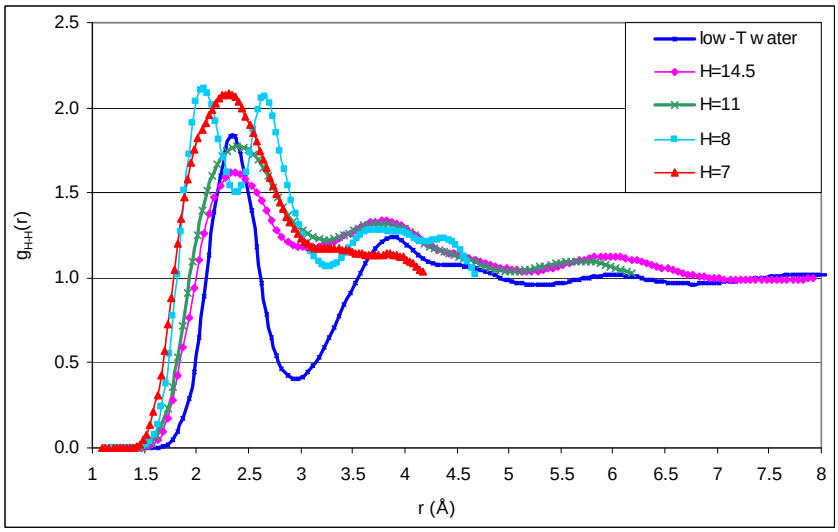

Figure 3.5. Continued.

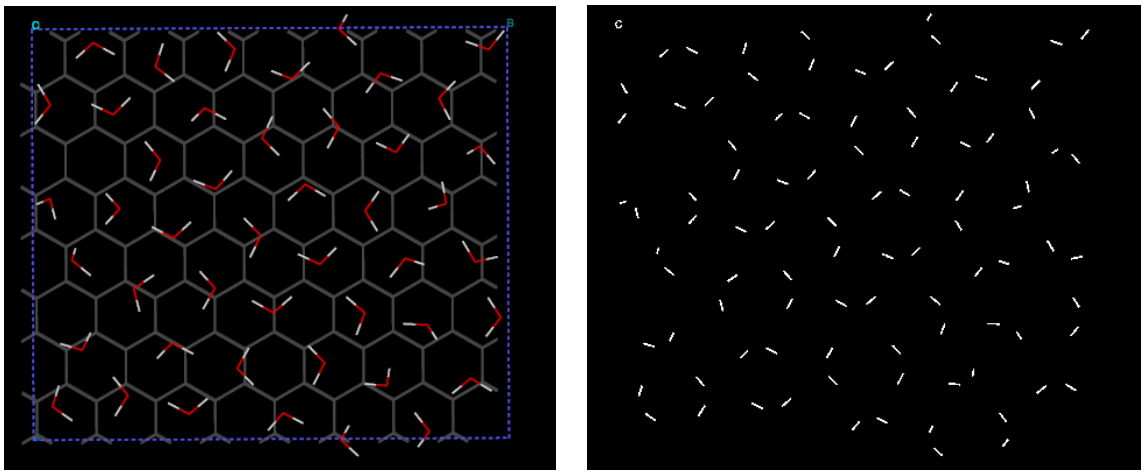

Figure 3.6. Snapshots of the water layer in contact with one of the walls for H = 8 Å. In the figure at the right, the background surface has been removed to visualize the order of the water structure.

An investigation was performed to determine at which temperature the water confined in the slit pores of H = 7 Å would have mobility comparable to low-temperature water. The results, shown in Figure 3.7, demonstrate that the temperature

has a mild effect on mobility in the confined system. At 323 K and 348 K, the time evolution of the MSD yields nearly the same slope as that at room temperature, thus indicating much lower mobility than bulk low-temperature water. It is at 373 K when the slope becomes similar to low-temperature water. It implies that the effect of the wall interaction exerted on confined water molecules produces a strong effect on the water dynamics which is disrupted only at very high temperatures.

Further insights into the dynamics of the system are obtained by analysis of the normalized velocity autocorrelation function (vacf) [17], defined as equation (2.6). The vacf of water molecules is computed in the lateral (x-y) direction. The results shown in Figure 3.8 again offer evidence of a clear difference between the dynamic behavior of bulk low-temperature water and confined water at the same density. The first minimum which corresponds to backscattering of the atoms becomes much deeper in the confined system as a consequence of its enhanced rigidity, as has been found in previous simulations of similar systems [37]. In the case of low-temperature water the first minimum is followed by an oscillation which is attributed to the intermolecular O-O stretch vibration, where the two water molecules are linked by H-bond [38]. Figure 3.8 shows that for H =14.5 Å, the vacf tends to become qualitatively similar to that of bulk water. However, at stronger confinements the number of oscillations and the depth of the first minimum increase, signaling restricted molecular mobility.

Vibrational (power) spectra obtained by Fourier transforming the vacf are displayed in Figure 3.9. The spectrum corresponding to low-temperature water has two characteristic features: a peak at low frequencies (centered at ~50 cm^{-1}) representing the O···O···O intermolecular bending motions of H-bonded molecule [39], and a shoulder at ~225 cm^{-1} resulting from the O···O intermolecular stretching mode, also related to the H-bond in bulk water. Such spectrum is substantially modified for confined water (Figure 3.9): the first peak has a blue shift (to higher frequencies) which becomes more pronounced as the separation between surfaces decreases. This may be another consequence of the distortion of the tetrahedral order caused by lateral diffusion being

reduced and also by changes in the distribution of H-bonds. The blue shift was also observed in interfacial water present in micellar solutions [39].

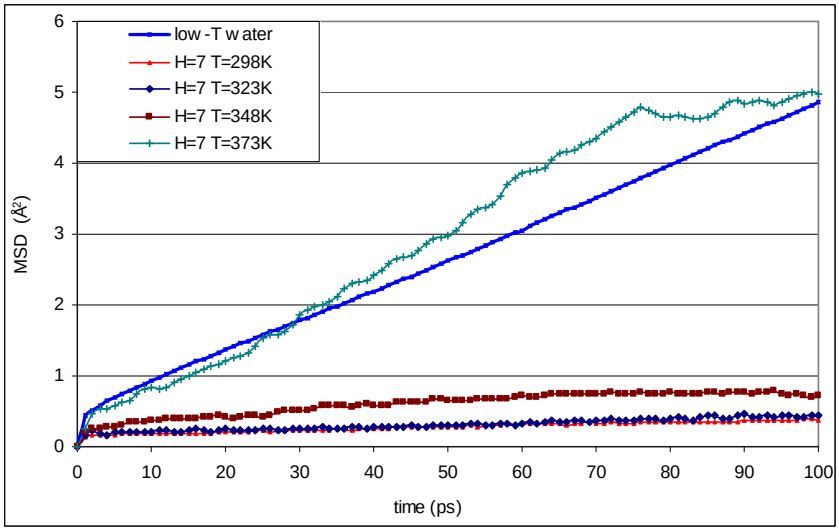

Figure 3.7. MSD of low-temperature water (213 K) and confined water in a pore of H = 7 Å at various temperatures.

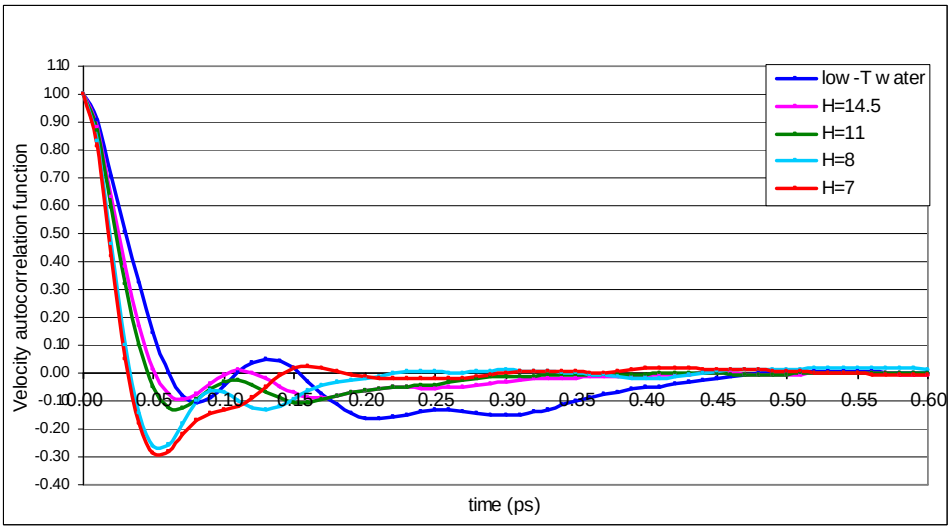

Figure 3.8. Velocity auto-correlation function of water molecules in low-temperature water, and that of water confined in slit pores separated 7, 8, 11, and 14.5 Å respectively.

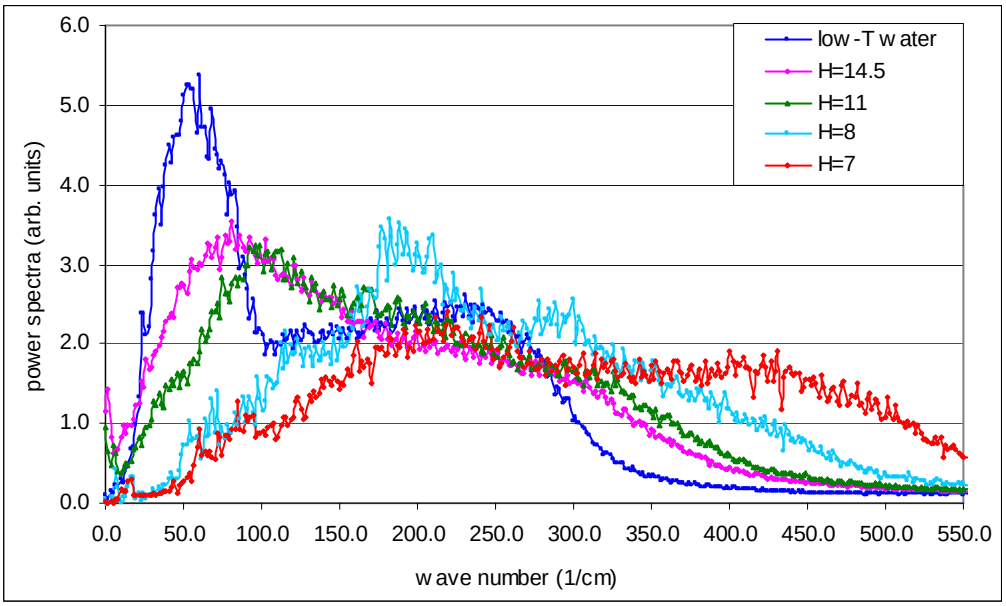

Figure 3.9. Power spectra obtained as the Fourier transform of the velocity auto-correlation function for water molecules in low-temperature water, and for water confined in slit pores separated 7, 8, 11, and 14.5 Å respectively.

3.2. Theoretical characterization of the structures of water clusters on a model graphite surface and confined within model graphite surfaces using ab initio simulations

3.2.1. Water clusters on a graphite surface

Optimized geometries of the benzene-$(H_2O)_n$ (n = 1-4) clusters are obtained from the MP2 calculations using the 6-31g(d) basis set.

3.2.1.1. (Benzene)-(H_2O)

The optimized geometries of one water molecule interacting with one benzene ring, and with two benzene rings are shown in Figure 3.10.

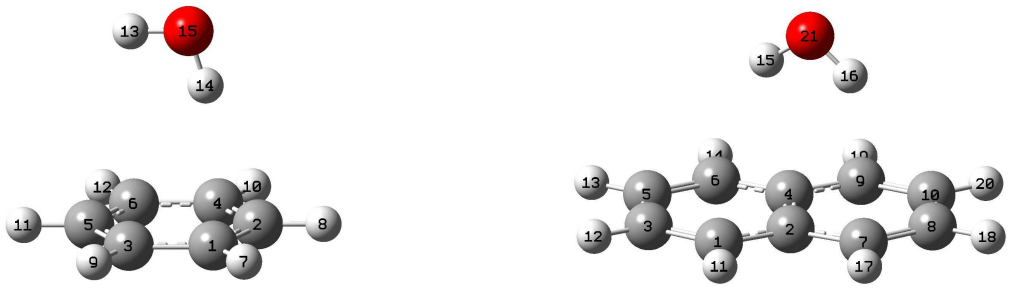

(a) (b)

Figure 3.10. Optimized structures of a water molecule interacting with: (a) one benzene ring, (b) two benzene rings.

Figure 3.10(a) shows that one of the O-H bonds of the water molecule points to a carbon atom of the benzene ring, and the other O-H bond is nearly parallel to the benzene ring. Qualitatively, these results agree with both theoretical [14, 40, 41] and experimental works by others [22, 23]. The distance between the oxygen atom and the benzene center-of-mass is 3.3 Å, while higher level theoretical calculations at both CCSD(T)/aug-cc-pVDZ and MP2/aug-cc-pVDZ levels of theory give distances of 3.23 and 3.211 Å [41]. Also, the results are in good agreement with the experimentally determined value of 3.32 Å [22, 23]. The distance from the center of benzene ring to the hydrogen atom bonded to the ring is 2.5 Å, while higher level theoretical calculations at both CCSD(T)/aug-cc-pVDZ and MP2/aug-cc-pVDZ levels of theory yield distances of 2.417 and 2.414 Å [41].

In the case of two benzene rings shown in Figure 3.10(b), both O-H bonds point to neighboring carbon atoms in qualitative agreement with MP2/aug-cc-pVDZ results [40]. The oxygen atom is above the surface at a distance of 3.0 Å, measured as the shortest vertical distance from the oxygen atom to the surface, slightly different from the value of 3.06 Å determined from MP2/aug-cc-pVDZ [40] using seven benzene rings interacting with one water molecule. It is found that the optimized geometries obtained by the MP2 calculations using the 6-31+g(d) basis set are in good agreement with those predicting by larger basis sets.

3.2.1.2. (Benzene)-$(H_2O)_2$

The optimized structures of a water dimer on one graphite surface represented by one benzene ring and two benzene rings are shown in Figure 3.11.

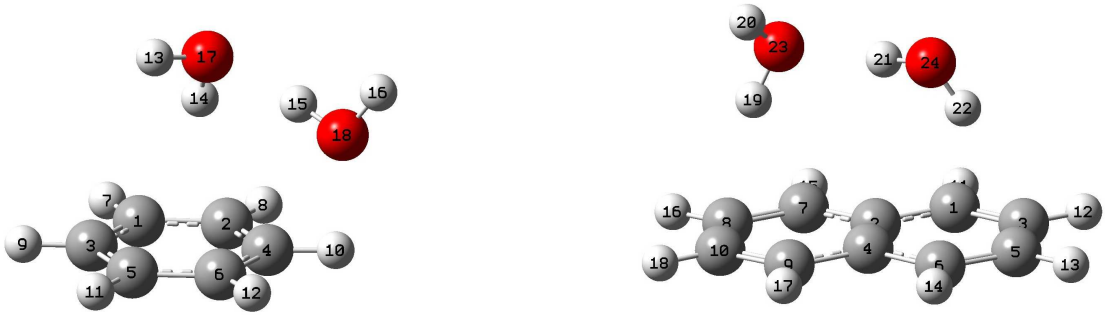

(a) (b)

Figure 3.11. Optimized structures of two water molecules interacting with: (a) one benzene ring, (b) two benzene rings.

As shown in Figure 3.11(a), one O-H points to the surface similarly to the case of one water molecule. Yet, the second water molecule is rather free from the surface and both of its O-H bonds point upward, forming one hydrogen bond with the other water molecule. The hydrogen bond length is 1.92 Å slightly shorter than the results from MP2/6-31+G(d,2p), 1.93 Å [14]. The O…O separation is 2.89 Å which is close to the value of 2.94 Å calculated from QCISD/6-31+G(d,2p) [14]. The hydrogen bond length of the complex is 0.034 Å shorter than that of an isolated water dimer [14]. Therefore, the water-water interaction is slightly stronger on the graphite surface. The O-H bond length associated with the hydrogen atom bonded with the surface is 0.976 Å, i.e. only 0.002 Å longer than for one water molecule. In addition, the distance of 2.43 Å between the center of the ring and the hydrogen atom bonded to the ring is 0.007 Å shorter than that in the case of one water molecule. These results suggest a slightly stronger attachment to the surface in the case of two water molecules than for one water molecule, in agreement with a report [14] using MP2/6-31+G(d,2p).

Figure 3.11(b) shows the optimized structure when increasing the surface to two benzene rings. Two O-H bonds from both water molecules, O_{23}-H_{19} and O_{24}-$H_{22,}$ point down to the surface. One O-H, O_{23}-$H_{20,}$ points away from the surface and O_{23}…H_{21} forms a hydrogen bond with the other water molecule. Thus, both water molecules interact with the surface and with each other. The hydrogen bond length is 1.93 Å which is 0.02 Å shorter than that of the isolated water dimer and 0.015 Å longer than the case of the surface of one benzene ring. The O…O separation distance is 2.90 Å, only 0.005 longer than for the interaction with one benzene ring. The distance between O_{23} and the surface is 3.15 Å, and between O_{24} and the surface is 3.26 Å, showing that the linear dimer is nearly parallel to the model surface. However, this parallel characteristic is not found in the case of the surface modeled by one benzene ring (Figure 3.11(a)). Although the structure of $(Benzene)_7$-$(H_2O)_2$ obtained by DFTB-D [40] shows a similar result to ours (where the linear dimer is nearly parallel to the surface) such structure differs in that there is only one O-H pointing to the surface. Our results are in good agreement with that found in QM/MD simulations using ONIOM(B3LYP/6-31+G(d):DFTB-D) [42].

3.2.1.3 (Benzene)-$(H_2O)_3$

Figure 3.12(a) shows the optimized geometry of three water molecules interacting with one benzene ring. The interaction of the trimer with the model surface is similar to that of the dimer and one benzene ring. There is only one O-H pointing to the surface. The other two water molecules are free from the surface but all of three water molecules form a cyclic network of hydrogen bonds. The hydrogen bonds are O_{17}…H_{15}, O_{17}…H_{21} and O_{20}…H_{16} with distances of 2.21, 1.95 and 2.13 Å, respectively. The distance between O_{17} and the surface is 2.70 Å, and between O_{18} and the surface is 2.17 Å, indicating that the O…O line is not parallel to the graphite surface. This may be because the water molecule, $H_{16}O_{18}H_{15}$, does not interact to the benzene ring. For this reason, the simulations of water clusters confined within model graphite surfaces which are discussed later have been done using two benzene rings representing a surface. The distance between the center of the benzene ring and the hydrogen atom associated to the

surface is 2.44 Å, which is 0.01 Å longer than for the case of two water molecules but 0.06 Å shorter than for the case of one water molecule. This suggests that the interaction between the water cluster and the model graphite surface is strongest for two water molecules, of intermediate strength for three water molecules, and less strong for one water molecule. This trend agrees with the MP2/6-31+G(d,2p) calculations by Fredericks and Jordan [14].

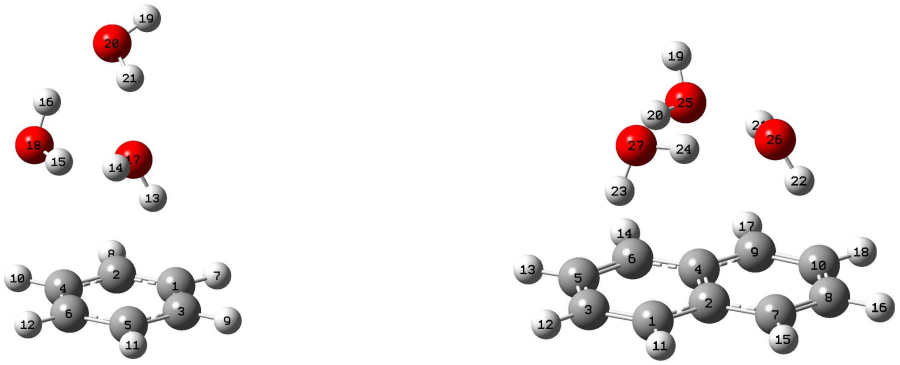

(a) (b)

Figure 3.12. Optimized structures of (a) one surface of one benzene ring interacting with three water molecules (b) one surface of two benzene rings interacting with three water molecules.

Figure 3.12(b) shows the optimized structure of two benzene rings interacting with three water molecules. The interaction of the trimer with the model graphite surface is slightly different from the case of one benzene ring but similar to the case of two benzene rings interacting with two water molecules. Two O-H from two water molecules, O_{26}-H_{22} and O_{27}-H_{23}, point down to the surface and one O-H, O_{25}-H_{19}, points away from the surface. A cyclic network of hydrogen bonds forms with O_{26}…H_{24}, O_{27}…H_{20} and O_{25}…H_{21}. The same configuration also has been found in $(Benzene)_7$-$(H_2O)_3$ using DFTB-D [40]. The distance between O_{25} and the surface is 2.81 Å,

between O_{26} and the surface is 3.08 Å and between O_{27} and the surface is 3.17 Å. Unlike the case of one benzene ring, these results indicate that the linear trimer is nearly parallel to this model graphite surface and similar to the case of the water dimer. These results are in agreement with our molecular dynamics simulation results shown in Figure 3.2.

3.2.1.4. (Benzene)-$(H_2O)_4$

Figure 3.13(a) shows two O-H pointing toward the surface and the other two O-H pointing away from the surface. All of four water molecules form a cyclic network of hydrogen bonds. The hydrogen bond distances, $O_{21}…H_{17}$, $O_{23}…H_{16,}$ $O_{22}…H_{20}$ and $O_{24}…H_{14}$, are 1.79, 1.82, 1.79 and 1.84 Å, respectively. The distance between O_{23} and the surface is 4.38 Å, and between O_{24} and the surface is 2.55 Å. This indicates that the top water molecule does not lay parallel to the graphite surface, which is similar to the cases of dimer and trimer. The distance between the center of the benzene ring and the hydrogen atom associated to the surface is 3.08 Å, which is 0.58 Å longer than the case of one water molecule in which the water cluster has the weakest interaction with the graphite surface. Therefore, the cluster of four water molecules has the weakest interaction with the graphite sheet compared to the cases of one, two and three water molecules. Furthermore, all the O…O distances are approximately of 2.8 Å. The tetramer is has a square shape linked by four hydrogen bonds but the four water molecules are not on the same plane as found in the case of the surface modeled by two benzene rings.

Figure 13.3(b) shows that the interaction of the water tetramer with the graphite surface is similar to the cases of dimer and trimer. The configuration exhibits two O-H, O_{17}-H_1 and O_{20}-H_8, from two water molecules pointing down to the surface and two O-H, O_{18}-H_4 and O_{19}-H_6, pointing away from the surface. Also, it shows a cyclic network of hydrogen bonds of $O_{17}…H_5$, $O_{19}…H_3$, $O_{18}…H_7$ and $O_{20}…H_2$. The linear tetramer is parallel to the model surface as shown by the distances of 2.43, 2.98, 3.50 and 3.31 Å between O_{17}, O_{18}, O_{19} and O_{20} and surface atoms, respectively. This structure also has been found in $(Benzene)_7$-$(H_2O)_4$ using DFTB-D calculation [40]. Moreover, the

configuration of the tetramer is a square and all the O…O distances are approximately 2.8 Å.

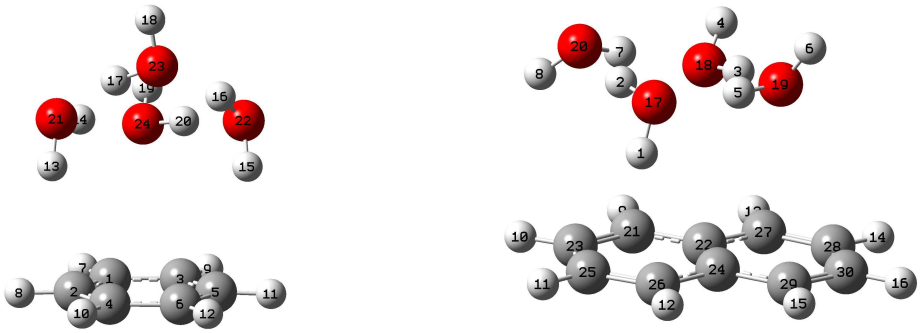

(a) (b)

Figure 3.13. Optimized structures of four water molecules interacting with: (a) one benzene ring and (b) two benzene rings.

3.2.2. Water clusters confined within model graphite surfaces

The initial configuration was constructed by adding a graphite surface parallel to the other surface in the converged configurations of water clusters interacting with a model graphite sheet. In the optimization process, the water molecule and the z coordinates of benzene which reflect the distance between the two surfaces were allowed to move freely (case A). Yet, the x and y coordinates of benzene are fixed. The surface represented by 2 benzene rings was chosen to perform optimization so that all water molecules are influenced by the confinement. The optimized geometries obtained using MP2/6-31G (d) calculations are shown in Figure 3.14.

The configuration of a water dimer, $(H_2O)_2$, confined within the model graphite surfaces is different from the case of water clusters interacting with one surface. Figure 3.14(a) shows that only one O-H points to the lower surface and one O-H points to the upper surface while the other two O-H are parallel to the surfaces as well as the oxygen atoms. However, there are two O-H pointing to the surface in the case of one surface.

This is because the confined system tends to form a symmetric structure. The O_{41}, O_{42}, H_{31} and H_{32} are approximately at the same distance of 2.96 Å to the surfaces. The distance between the oxygen atoms (Table 3.1) are 0.031 Å shorter and the hydrogen bond is 0.04 shorter from the case of one surface. Therefore, water-water interaction is slightly stronger in the confined environment. The average distance of O...surface and H...surface are approximately 0.06 and 0.31 Å shorter than the case of only one surface. Thus, the interaction between water molecules and the graphite surface are also stronger due to the confinement. The distance from the oxygen atoms to the upper and the lower surfaces are approximate equally at 3 Å while the distance between the surfaces are approximately 5.99 Å. Thus, the O_{41}, O_{42}, H_{31} and H_{32} atoms locate at the middle between the graphite surfaces. The structure in Figure 3.14(a) shows two O-H bonds belonging to O_{42} are parallel to the surface. This satisfies one of the preferential orientations of water molecules that both O-H bonds are parallel to the surface as the results of the reported structures from the MD simulation.

A water trimer between two surfaces shows the same arrangements as does the case with one surface (Figure 3.14(b)). One O-H bond of each water molecule points to the surface and hydrogen bonds are maximized by forming a cyclic network of them. As shown in Table 3.2, the distance between O…O and hydrogen bonds length are slightly shorter than the case of one surface, showing a littler stronger interaction between water molecules under a confinement environment. Also, the results of approximately 0.028 and 0.15 Å shorter O...surface and H...surface distances, compared to the case of one surface, suggest a stronger interaction between water molecules and the model graphite surface under a confinement environment. The average distance between the two surfaces is 6.66 Å and the oxygen atoms are approximately located in the middle between the graphite surfaces. (Approximately 3.1 Å between oxygen atoms and the lower and upper surfaces).

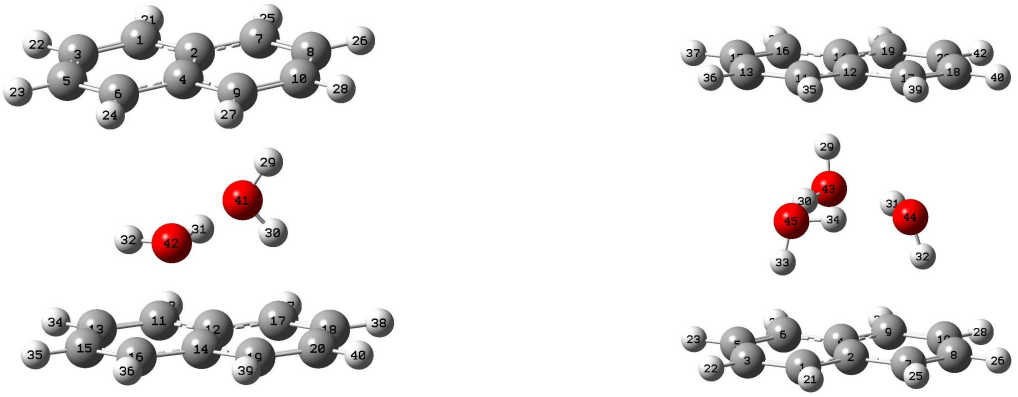

(a)

(b)

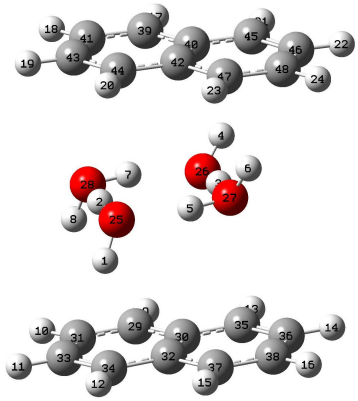

(c)

Figure 3.14. The optimized structures of water molecules confined within two surfaces of graphite (a) $(H_2O)_2$ (b) $(H_2O)_3$ (c) $(H_2O)_4$. During the optimization process, water molecules and z coordinates of benzene are allowed to move freely but the x, y coordinates of benzene are fixed.

Figure 3.14(c) shows that a water tetramer between two graphite surfaces locates in the same arrangements as is the case with one surface and two O-H pointing down, two O-H pointing away from one of the surfaces and a square cyclic network of hydrogen bonds is formed. These square cycles of hydrogen bonds were also found in the MD simulations as shown in Figure 3.2(left) maximizing hydrogen bonds. However, the configuration of two O-H bonds pointing down and two O-H bonds pointing away

from one of the surfaces has not found in the MD results. This might be because the models of graphite surfaces in the MD are larger. The complex shows a symmetric geometry. All O…O distances and hydrogen bond lengths are shorter than in the case of one surface (Table 3.1), indicating that water-water interaction in confinement is stronger, similarly to the case of one, two and three water molecules. The distance between the two surfaces is 6.87 Å and the oxygen atoms are approximately 3.4 Å from the lower and upper surfaces. The average 0.068 and 0.101 Å shorter O...surface and H...surface distances, compared to the case of one surface, indicates a stronger interaction between water molecules and the model graphite surface under a confinement environment.

Two from eight O-H of four water molecules point to the surface while four are parallel to the surface and two point away from the surface, indicating that they tend to be parallel to the graphite surface and maximize the hydrogen bonds rather than pointing toward the surface. This agrees with the findings in the MD simulations with bulk water (Figure 3.2). These results also support those found in the MD simulations that there are some hydrogen atoms located closer to the graphite surface than the corresponding oxygen atoms as shown in Figure 3.3. According to the reported structures from the MD simulation results, the structure shown in Figure 3.14(b) and (c) present one of the preferential orientations of water molecules with one O-H pointing to the surface and the other parallel.

Thus, water clusters confined within model graphite surfaces show symmetric configurations and the oxygen atoms locate approximately in the middle between the surfaces. At least one O-H bond of each water molecule is parallel to the surface. A cyclic network of hydrogen bond is formed because the system tries to maximize hydrogen bonds. Water-water interaction between two surfaces is stronger than in the case of one surface and the water-graphite interaction is stronger as well. The distance between the surfaces increases with the number of water molecules. The MP2 calculations present both of the preferential orientations of water molecules as reported in the MD simulation results that one O-H pointing to the surface and the other parallel

and that both O-H bonds parallel to the surface. Moreover, Lin et al [40] have shown that both orientations of water molecules present in the system of one surface of $(Benzene)_7$ interacting to $(H_2O)_6$.

In the case of one water molecule confined between the two surfaces, as the program is performing the optimization, the structure changes in a way such that the water molecule tries to escape from the confined space. The program cannot optimize the system of one water molecule confined between the two surfaces.

Furthermore, the initial configurations of water clusters confined in the graphite surfaces were optimized by allowing z coordinates of every atom to move but restricting x, y coordinates of every atom (case B). This means that the optimized structures of water clusters interacting with a graphite surface are fixed but the distances between them and the two surfaces are optimized. Comparing the distances between the two surfaces of the two different optimization constraints, the values are slightly different as shown in Table 3.2. The distances increase with the number of water molecules for both cases but case B gives higher distance values. Also, the oxygen atoms locate approximately at the middle between the surfaces similarly to the case of water molecules moving freely. However, the energy values of this method are higher.

Table 3.1. Distances in Å of water clusters on a graphite surface and water clusters confined within graphite surfaces.

Distance, Å	$(H_2O)_2$		$(H_2O)_3$		$(H_2O)_4$	
	1 surface[a]	2 surfaces	1 surface[a]	2 surfaces	1 surface[a]	2 surfaces
O…O	2.897	2.866	$O_{25}..O_{26}$, 2.862 $O_{26}..O_{27}$, 2.811 $O_{25}..O_{27}$, 2.797	$O_{43}..O_{44}$, 2.827 $O_{44}..O_{45}$, 2.813 $O_{45}..O_{43}$, 2.797	$O_{17}..O_{19}$, 2.744 $O_{19}..O_{18}$, 2.772 $O_{18}..O_{20}$, 2.792 $O_{20}..O_{17}$, 2.807	$O_{25}..O_{27}$, 2.697 $O_{27}..O_{26}$, 2.668 $O_{26}..O_{28}$, 2.702 $O_{28}..O_{25}$, 2.731
O…H (hydrogen bonds)	1.931	1.891	$O_{27}..H_{20}$, 1.872 $O_{25}..H_{21}$, 1.977 $O_{26}..H_{24}$, 1.920	$O_{45}..H_{30}$, 1.872 $O_{43}..H_{31}$, 1.913 $O_{44}..H_{34}$, 1.898	$O_{17}..H_5$, 1.762 $O_{19}..H_3$, 1.797 $O_{18}..H_7$, 1.816 $O_{20}..H_2$, 1.841	$O_{25}..H_5$, 1.717 $O_{27}..H_3$, 1.679 $O_{26}..H_7$, 1.722 $O_{28}..H_2$, 1.764
O...surface	O_{23}, 3.147 O_{24}, 3.259 Avg, 3.203	O_{42}, 3.0491 O_{41}, 3.228 Avg, 3.139	O_{25}, 3.080 O_{26}, 3.169 O_{27}, 3.169 Avg, 3.139	O_{43}, 3.167 O_{44}, 3.056 O_{45}, 3.111 Avg, 3.111	O_{17}, 3.431 O_{18}, 2.985 O_{19}, 3.498 O_{20}, 3.610 Avg, 3.513	O_{25}, 3.489 O_{26}, 3.355 O_{27}, 3.534 O_{28}, 3.400 Avg, 3.445

Table 3.1. Continued.

Distance, Å	$(H_2O)_2$		$(H_2O)_3$		$(H_2O)_4$	
	1 surface[a]	2 surfaces	1 surface[a]	2 surfaces	1 surface[a]	2 surfaces
H...surface	H_{19}, 2.500 H_{22}, 2.656 Avg, 2.578	H_{29}, 2.279 H_{30}, 2.255 Avg, 2.266	H_{22}, 2.545 H_{23}, 2.589 Avg, 2.567	H_{29}, 2.389 H_{32}, 2.389 H_{33}, 2.472 Avg, 2.417	H_1, 2.697 H_8, 3.000 Avg, 2.843	H_1, 2.563 H_8, 2.563 H_4, 2.921 H_6, 2.721 Avg, 2.742

[a] water clusters on a graphite surface represented by two benzene rings.

Table 3.2. Average distances between the two surfaces, unit Å.

	$(H_2O)_2$	$(H_2O)_3$	$(H_2O)_4$
Case A	6.0	6.7	6.9
Case B	6.4	6.9	7.0

Additional geometry optimizations were performed without any constraints. The optimal geometries are shown in Figure 3.15. The arrangements of water clusters are similar to the case of only one surface and the surfaces tend to arrange forming a T-shaped structure, which is one of the preferred configurations of the benzene dimer [20, 43-45]. Therefore, the surface tends to interact with the other surface as well as with water clusters.

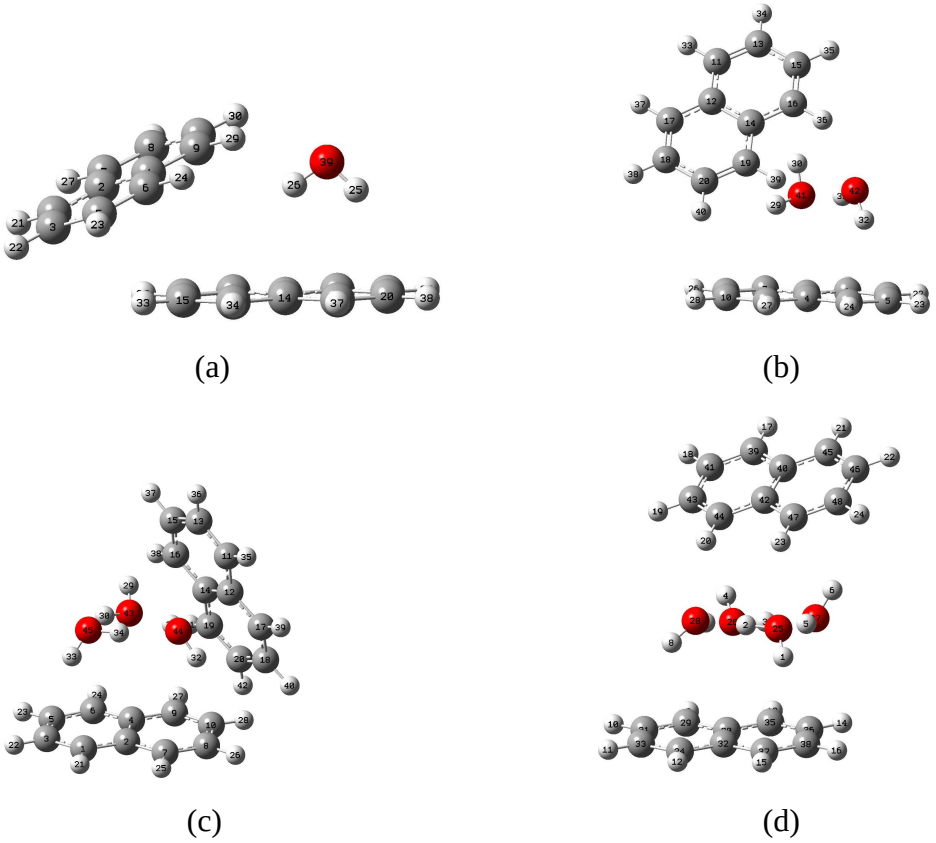

(a) (b)

(c) (d)

Figure 3.15. The optimal structures without constraints (a) H_2O (b) $(H_2O)_2$ (c) $(H_2O)_3$ (d) $(H_2O)_4$.

3.3. Proton transfer between two water molecules confined within the graphite surfaces

The initial configuration of a hydronium ion and a water molecule confined within the graphite surfaces was optimized using MP2/6-31G(d) under the constraints that the hydronium ion, the water molecule, and the z coordinates of the surfaces were allowed to be varied. However, the x and y coordinates of the surfaces were restricted. The optimal geometry is shown in Figure 3.16. At the beginning, H_{39} was the hydrogen atom from the hydronium ion and belonged to O_{43}. The optimum distances between the oxygen atoms (R_1) and R_2, are 2.42 and 1.21 Å, respectively. The separation distance

between the surfaces, H, is 5.89 Å. The oxygen atoms and H^+ locate at the middle between the surfaces and parallel to them.

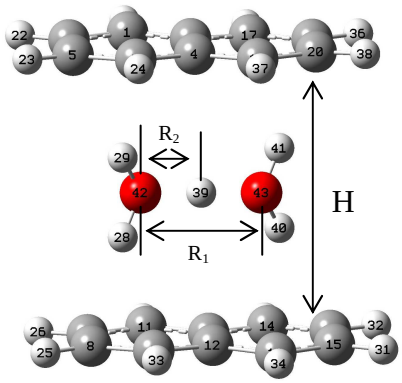

Figure 3.16. Optimal structure of H_3O^+-(H_2O) confined within the graphite surfaces.

The energy barriers for proton transfer from a hydronium ion in a confined environment as the proton propagates along the O-H···O hydrogen bond direction of the H_3O^+-(H_2O) complexes were determined. The distances R_1 were scanned at various H of 4, 6, 8, 10, 14.5 and 20 Å using the optimized geometry. The energy barrier (Table 3.3) is defined as the energy difference between the maximum and minimum points of the curve (Figure 3.17-3.22). At a specific R_1, the maximum points give an estimate of the transition state of proton transfer. The left minimum points denote the equilibrium of a left H_3O^+ with a right H_2O. The symmetric minimum points at the right denote the equilibrium of a right H_3O^+ with a left H_2O. As shown in Figure 3.17-3.22, only when R_1 is at the optimal distance (R_1=2.42 Å), the curves show a single minimum for every varied H. Also, all other R_1 curves show symmetric double-well shapes similar to those found in the H_3O^+-(H_2O) complexes in the unconfined environment [24]. Figure 3.23 shows that at a specific R_1 the system energy is increasing as H is increasing but it shows a very small change at H = 14.5 and 20 Å. However, it rapidly increases when H is decreased to H = 4 Å. Considering Table 3.3, as R_1 increases, the energy barrier

increases very sharply for every value of H. The energy barriers at H = 4 Å are the highest in every R_1 distance and increase sharply compared to the other H values and non-confinement. The energy barriers at H = 6 Å for every varied R_1 are very close to those of the case of no confinement. At a specific R_1, when H is increasing between 6-14.5 Å, the energy barrier decreases. However, the energy barriers start increasing when H increases from 14.5 to 20 Å. The results suggest an interesting possibility that the confinement environment can either reduce or raise the barrier energy of proton transfer. At H = 4 Å, the H_3O^+-(H_2O) complexes strongly interact with the surfaces. This might result in a higher energy requirement for a proton to overcome that strong interaction and to be transported from one molecule to another. The interaction energy of the simple example system of H_3O^+ confined between the two model graphite surfaces has been calculated by subtracting the total energy of the system from the energy of H_3O^+, H_2O and the surfaces. The results as shown in Table 3.4 show extremely strong interaction energy at H = 4 Å compared to the other H values. Additionally, it shows that at H = 6 Å, which is close to the optimum H, we find a very small value (1.44 kcal/mol) of interaction energy. Also, as H is increased from 6 Å, the interaction energy is increasing but it does not significantly increase when H is greater than 14.5 Å. Although the interaction energy is increasing between H = 6-25 Å, the energy barrier is reduced and starts to increase at H = 20 Å. Therefore, it suggests that at a specific range of surface separation between 6-14.5 Å the confinement effect somehow plays an important role on the proton transportation which does not only help to defeat the increasing interaction energy of the system but also creates even less energy barrier than the system of the least interaction energy (H=6 Å). Nevertheless, the confinement does not make proton transfer easier when H is greater than 14.5 Å as the barrier energy begins to increase. It should be noted that the barrier energy has been calculated when the H_3O^+-(H_2O) complexes are located in the middle between the surfaces. Thus, it implies that the complex does not feel the walls when H is greater than 14.5 Å. It can be seen in Figure 3.2 that at H=14.5 Å water molecules located in the middle (layer 2 and 3) are not well ordered.

Table 3.3. Energy barriers for proton transfer of the system shown in Figure 3.16 in kcal/mol.

R_1 (Å)	No confinement	Confined within the model graphite surfaces					
		H = 4 Å	H = 6 Å	H = 8 Å	H = 10 Å	H = 14.5 Å	H = 20 Å
2.55	0.659	1.780	0.792	0.594	0.526	0.502	0.498
2.6	1.491	2.950	1.678	1.387	1.287	1.249	1.252
2.7	3.950	6.480	4.209	3.743	3.591	3.533	3.535
2.8	7.223	10.762	7.544	6.915	6.710	6.634	6.635
2.9	11.111	15.768	11.516	10.732	10.460	10.375	11.111
3.1	20.211	27.229	20.866	19.699	19.316	19.222	19.188

Table 3.4. Interaction energy of the H_3O^+ confined within the two model graphite surfaces (kcal/mol).

H (Å)	Interaction energy (kcal/mol)
4	137.182
6	1.438
8	21.604
10	33.582
14.5	43.177
20	45.520
25	46.233

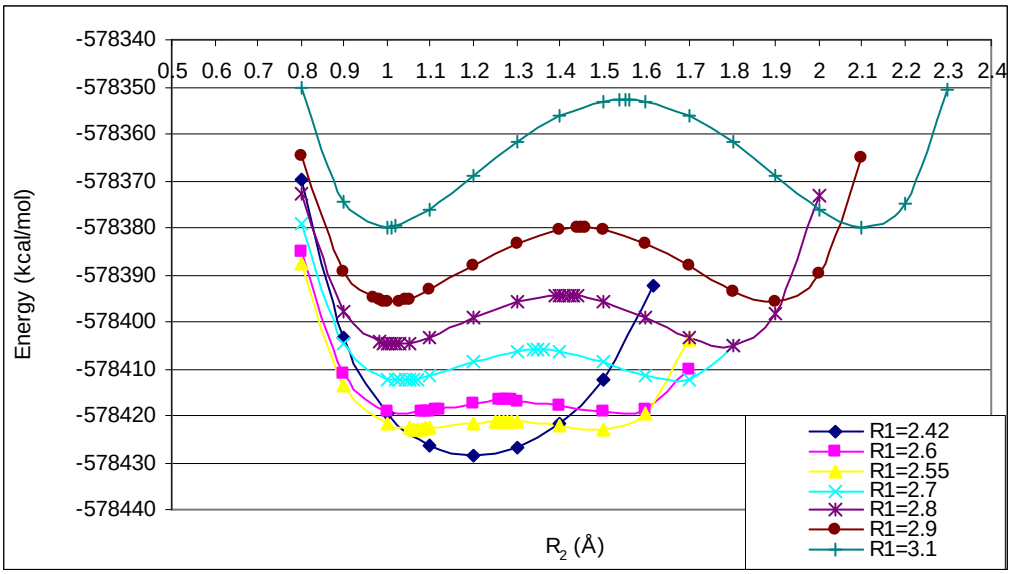

Figure 3.17. Energy of the system shown in Figure 3.16 at H = 4 Å.

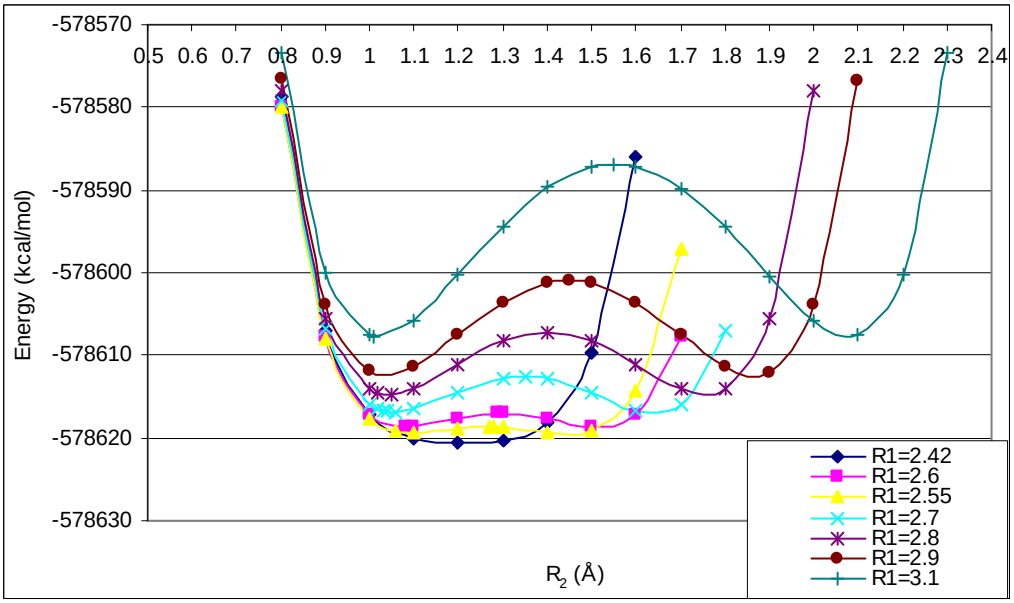

Figure 3.18. Energy of the system shown in Figure 3.16 at H = 6 Å.

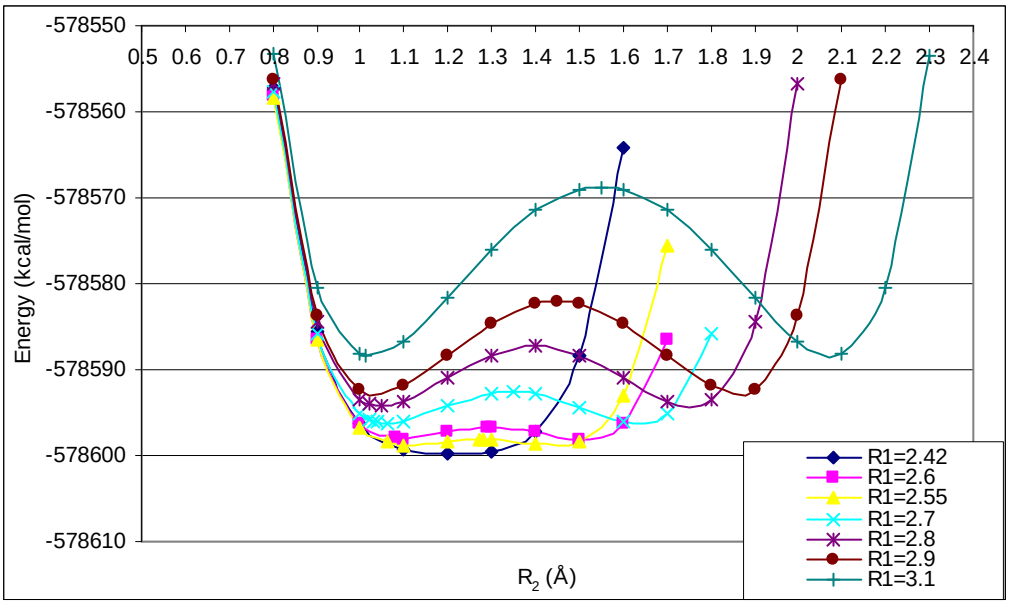

Figure 3.19. Energy of the system shown in Figure 3.16 at H = 8 Å.

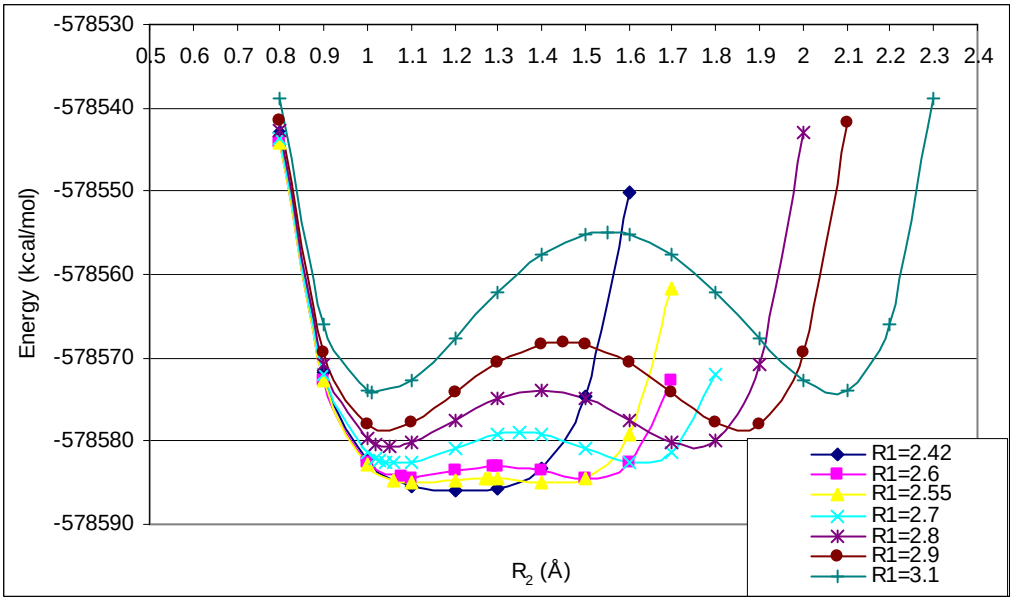

Figure 3.20. Energy of the system shown in Figure 3.16 at H =10 Å.

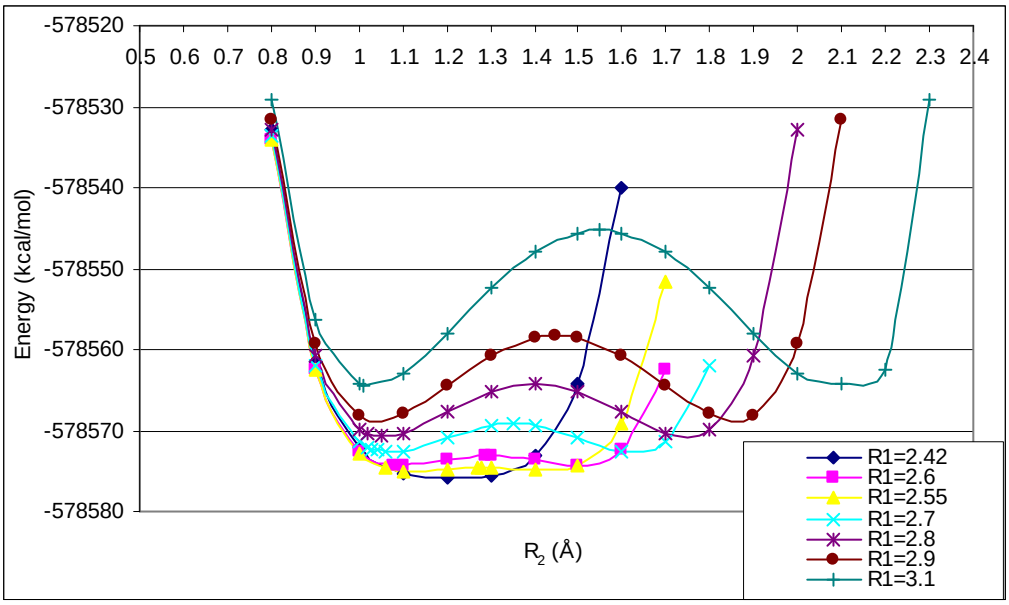

Figure 3.21. Energy of the system shown in Figure 3.16 at H =14.5 Å.

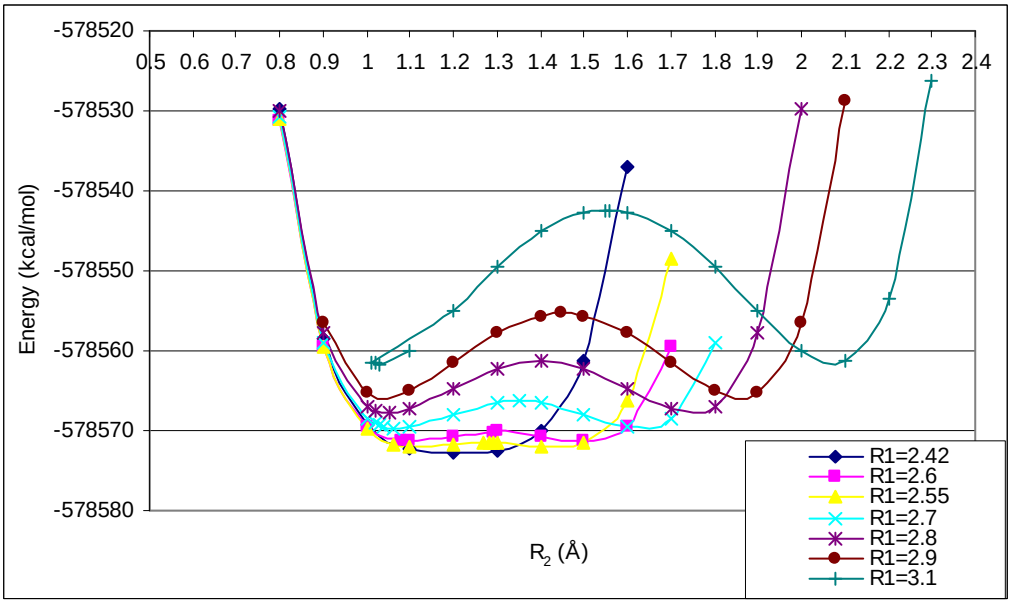

Figure 3.22. Energy of the system shown in Figure 3.16 at H =20 Å.

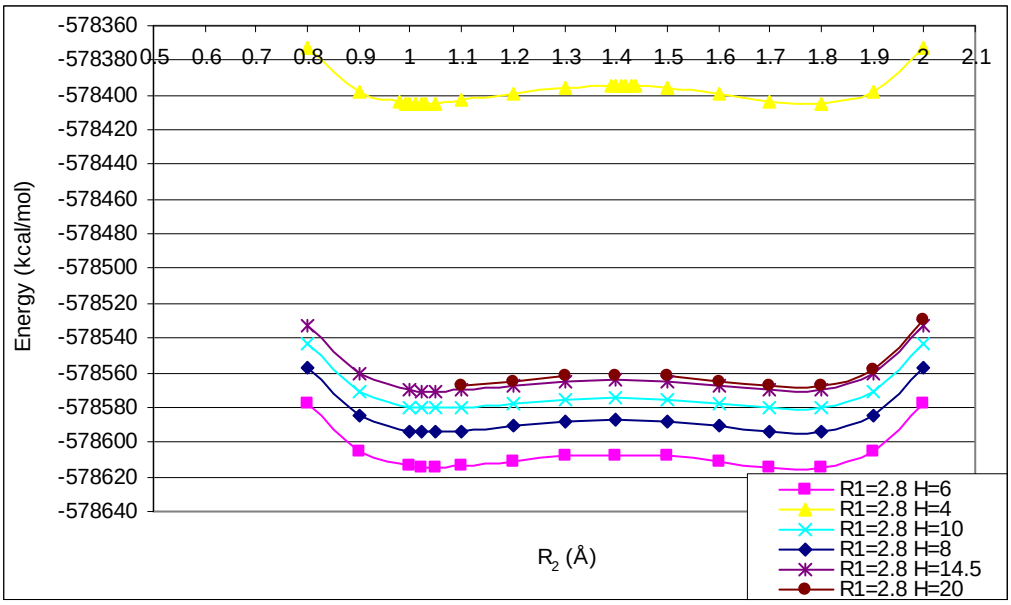

Figure 3.23. Energy of the system shown in Figure 3.16 at R_1 = 2.8 Å.

Furthermore, the barrier energy for proton transfer with another possible configuration of the H_3O^+-(H_2O) complexes has been studied. The optimization of the H_3O^+-(H_2O) complexes confined between the two model graphite sheets are performed at fixed H = 8 Å. The complexes tend to arrange as shown in Figure 3.24.

Unlike Figures 3.17-3.23, Figure 3.25 shows that the energy curves of every R_1 of the system, which are shown in Figure 3.24 at H = 8 Å, do not show the symmetric double wells shape due to the asymmetric configuration of the system itself. Considering Table 3.5, the calculated barrier energy shows the same trend with the energy barrier found in the configuration shown in Figure 3.16. As R_1 is increasing, the energy barrier increases for every varied H. The energy barrier decreases when H is increasing between 8-14.5 Å and it begins to increase at H = 20 Å. However, barrier energies shown in Table 3.5 are much higher than those shown in Table 3.3 at the same H and R_1.This result suggests that the arrangement shown in Figure 3.16 enhances proton transfer compared to the arrangement shown in Figure 3.24.

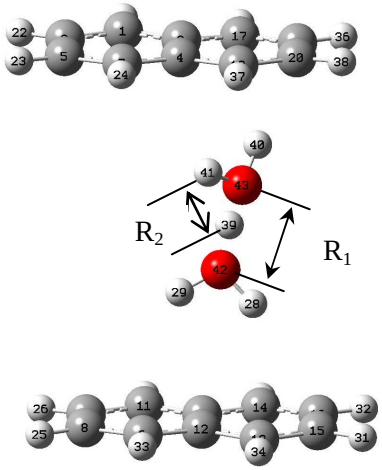

Figure 3.24. Another possible structure of H_3O^+-(H_2O) confined within the graphite surfaces.

Although the H_3O^+-(H_2O) complexes at H = 20 Å are located closer to the surfaces than the configuration shown in Figure 3.16, the confinement does not encourage the proton transfer as the energy barrier begins to increase. At H =20 Å, the complexes are approximately 8 Å from the surfaces (Figure 3.24 configuration) and 9.5 Å (Figure 3.16 configuration). The complexes in the Figure 3.16 configuration with H = 14.5 Å are located approximately 6.5 Å from the surfaces and the energy barriers decrease. Therefore, when the complexes are separated from the surfaces by more than 8 Å, the confinement ceases to benefit the proton transfer.

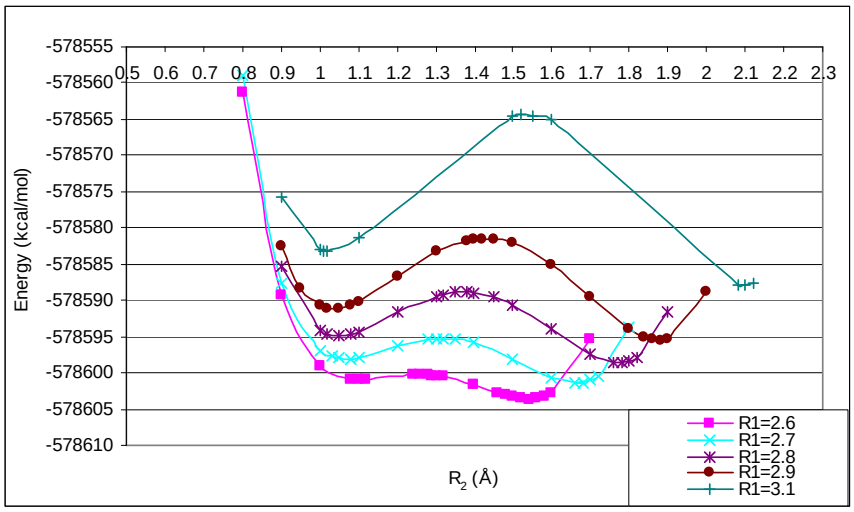

Figure 3.25. Energy of the system shown in Figure 3.24 at various R_1 and H = 8 Å.

Table 3.5. Energy barriers for proton transfer of the system shown in Figure 3.24 in kcal/mol.

R_1 (Å)	H = 8 (Å)	H = 10 (Å)	H = 14.5 (Å)	H = 20 (Å)
2.6	2.226	1.686	1.409	2.842
2.7	4.808	4.085	3.710	5.537
2.8	8.204	7.333	6.842	8.998
2.9	12.240	11.227	10.630	13.031
3.1	21.705	20.459	19.625	22.318

CHAPTER IV

CONCLUSIONS

MD simulations of water encapsulated in slit graphite pores reveal a well-ordered layered water structure in the horizontal direction parallel to the graphite surfaces. When the surfaces are separated by distances of less than 8 Å, keeping the water density constant, a compact frozen structure composed of two layers is obtained. The mobility is much lower than that of low-temperature water, and each water layer interacts strongly with its closest hydrophobic surface. Those water molecules in contact with the surface tend to orient their dipoles parallel to the surface. For larger separations, additional water layers are formed in the pore center, and the average diffusion coefficient increases, becoming larger than that of low-temperature water for separations greater than 8 Å. At H = 8 Å, confined water has similar mobility as bulk low-temperature water (213K); however it has a very different structure. At H =7 Å the water mobility is much lower than that of low-temperature water. The strong hydrophobic interaction between water molecules and graphite can be reduced by a large temperature increase, and the simulations indicate that the mobility of water molecules becomes similar to low-temperature water at 373 K in a pore of H = 7 Å. Structural and dynamical analyses suggest that the tetrahedral structure of low-temperature water is no longer present in the confined systems. Notable changes are observed in the intermolecular vibrational modes, mainly a blue shift of the O···O···O intermolecular bending motion which becomes more pronounced as the separation between walls becomes smaller, again signaling suppression of the tetrahedral order and increased system rigidity.

Nevertheless, the preliminary study using classical MD simulations did not include H…C interactions in the force field. Also, the obtained orientation of water molecules confined within the two graphite surfaces required a better understanding of the involved geometric and electronic effects. Therefore, an additional analysis of the geometry of water clusters using ab initio calculations has been performed in an attempt to get new insights regarding the structure and dynamics of confined water. The graphite model is represented by a benzene ring. The optimized geometries of $(H_2O)_n$ (n=1-4)

interacting with the graphite model are obtained by the ab initio MP2 and 6-31g(d) basis set. The results are in qualitative agreement with those results predicted by higher levels of theory and larger basis sets. The optimized geometries of the expanded graphite model using two benzene rings interacting to $(H_2O)_n$ (n = 2-4) exhibit slightly different arrangements from the case of using one benzene ring as a graphite model. They show that water molecules locate nearly parallel to the surface and form a cyclic network of hydrogen bonds. Two O-H bonds from two water molecules point down to the surface and at least one O-H bond points away from the surface for n = 2-4. Also, the water-water interaction is slightly stronger on the graphite surface than the isolated water molecules as the O…O separation and the hydrogen bond length are shorter.

Furthermore, the optimized geometries of $(H_2O)_n$ (n = 2-4) within model graphite surfaces (modeled as two benzene rings per surface) show fairly similar arrangements with the case of water clusters interacting with one surface. A cyclic network of hydrogen bonds are formed because the system attempts to maximize the number of hydrogen bonds. At least one O-H bond from one water molecule is parallel to the surfaces. The oxygen atoms locate approximately in the middle between the surfaces and are parallel to the surfaces. The optimized structures show that the confined system tends to form a symmetric structure. The MP2 calculations present the two most likely orientations of water molecules which are; 1) one O-H bond point to the surface and the other is parallel; 2) both O-H bonds are parallel to the surface. These orientations agree with those found in the MD simulation results. Also, water-water interaction between two surfaces is stronger than in the case of one surface as the O…O distance and the hydrogen bond length are shorter. The water-graphite interaction is stronger because O…surface and H…surface distances are shorter.

Additionally, the energy barriers for proton transfer from a hydronium ion in a confined environment were calculated as the proton propagates along the O-H···O hydrogen bond direction of the H_3O^+-(H_2O) complexes. The energy barriers were determined from the optimized configuration (Figure 3.16) of a hydronium ion and a water molecule confined within the graphite model surfaces using MP2/6-31G(d). As R_1

(the distance between two oxygen atoms) increases, the energy barrier increases very sharply for every varied H. At H = 6 Å, which is close to the optimal H (5.89 Å), the energy barriers are very close to those of the case of no confinement. The results show that as H is increased up to 14.5 Å, the energy barriers decrease but they begin to increase at H = 20 Å. Therefore, it can be concluded that a specific range of H which enhances the proton transfer is H = 6-14.5 Å. Also, when the system is highly confined at H = 4 Å, the energy barriers are extremely high due to very high interaction between the H_3O^+-(H_2O) complexes and the surfaces. Moreover, the energy barriers for proton transfer were determined from another possible configuration (Figure 3.24) of the H_3O^+-(H_2O) complexes confined within the graphite model surfaces. The energy barriers show the same trend as the other configuration but with much higher values. In addition, the confinement in this configuration does not enhance the proton transfer when the H_3O^+-(H_2O) complexes are located more than 8 Å from the surfaces which is manifested by an increase in the energy barriers at H = 20 Å.

REFERENCES

[1] J. K. Brennan, T. J. Bandosz, K. T. Thomson, and K. E. Gubbins, Colloids and Surfaces A: Physicochemical and Engineering Aspects **187-188**, 539 (2001).

[2] A. Striolo, K. E. Gubbins, A. A. Chialvo, and P. T. Cummings, Adsorption **11**, 337 (2005).

[3] T. Ohba, H. Kanoh, and K. Kaneko, Chemistry - A European Journal **11**, 4890 (2005).

[4] N. Choudhury, and B. M. Pettitt, J. Am. Chem. Soc. **127**, 3556 (2005).

[5] A. Striolo, A. A. Chialvo, K. E. Gubbins, and P. T. Cummings, J. Chem. Phys. **122**, 234712 (2005).

[6] A. Striolo, P. K. Naicker, A. A. Chialvo, P. T. Cummings, and K. E. Gubbins, Adsorption **11**, 397 (2005).

[7] T. Iiyama, K. Nishikawa, T. Otowa, and K. Kaneko, J. Phys. Chem **99**, 10075 (1995).

[8] T. Iiyama, K. Nishikawa, T. Suzuki, and K. Kaneko, Chem. Phys. Lett. **274**, 152 (1997).

[9] K. Koga, G. T. Gao, H. Tanaka, and X. C. Zeng, Nature **412**, 802 (2001).

[10] K. D. Kreuer, Chem. Mater. **8**, 610 (1996).

[11] C. Dellago, M. M. Naor, and G. Hummer, Phys. Rev. Lett. **90**, 105902 (2003).

[12] D. J. Mann, and M. D. Halls, Phys. Rev. Lett. **90**, 195503 (2003).

[13] N. Agmon, Chem. Phys. Lett. **244**, 456 (1995).

[14] S. Y. Fredericks, K. D. Jordan, and T. S. Zwier, J. Phys. Chem. **100**, 7810 (1996).

[15] D. Feller, and K. D. Jordan, J. Phys. Chem. A **104**, 9971 (2000).

[16] H. J. C. Berendsen, J. R. Grigera, and T. P. Straatsma, J. Phys. Chem. **91**, 6269 (1987).

[17] M. P. Allen, and D. J. Tildesley, Computer Simulation of Liquids (Oxford University Press, Oxford, 1990).

[18] W. A. Steele, The Interaction of Gases with Solid Surfaces (Pergamon Press, Oxford, 1974).

[19] W. Smith, and T. R. Forester, (Daresbury Laboratory, Daresbury, 1996).

[20] P. Hobza, H. L. Selzle, and E. W. Schlag, J. Phys. Chem. 100, 18790 (1996).

[21] M. J. F. Gaussian 03 Revision C.02, G. W. Trucks, H. B. Schlegel, G. E. Scuseria, M. A. Robb, J. R. Cheeseman, J. A. Montgomery, Jr., T. Vreven, K. N. Kudin, J. C. Burant, J. M. Millam, S. S. Iyengar, J. Tomasi, V. Barone, B. Mennucci, M. Cossi, G. Scalmani, N. Rega, G. A. Petersson, H. Nakatsuji, M. Hada, M. Ehara, K. Toyota, R. Fukuda, J. Hasegawa, M. Ishida, T. Nakajima, Y. Honda, O. Kitao, H. Nakai, M. Klene, X. Li, J. E. Knox, H. P. Hratchian, J. B. Cross, V. Bakken, C. Adamo, J. Jaramillo, R. Gomperts, R. E. Stratmann, O. Yazyev, A. J. Austin, R. Cammi, C. Pomelli, J. W. Ochterski, P. Y. Ayala, K. Morokuma, G. A. Voth, P. Salvador, J. J. Dannenberg, V. G. Zakrzewski, S. Dapprich, A. D. Daniels, M. C. Strain, O. Farkas, D. K. Malick, A. D. Rabuck, K. Raghavachari, J. B. Foresman, J. V. Ortiz, Q. Cui, A. G. Baboul, S. Clifford, J. Cioslowski, B. B. Stefanov, G. Liu, A. Liashenko, P. Piskorz, I. Komaromi, R. L. Martin, D. J. Fox, T. Keith, M. A. Al-Laham, C. Y. Peng, A. Nanayakkara, M. Challacombe, P. M. W. Gill, B. Johnson, W. Chen, M. W. Wong, C. Gonzalez, and J. A. Pople, (Gaussian, Inc., Wallingford CT, 2004).

[22] S. Suzuki, P. G. Green, R. E. Bumgarner, S. Dasgupta, W. A. Goddard III *et al.*, Science **257**, 942 (1992).

[23] H. S. Gutowsky, T. Emilsson, and E. Arunan, J. Chem. Phys. **99**, 4883 (1993).

[24] T. Li, A. Wlaschin, and P. B. Balbuena, Ind. Eng. Chem. Res. **40**, 4789 (2001).

[25] R. Garcia-Fernandez, J. L. F. Abascal, and C. Vega, J. Chem. Phys. **124**, 144506 (2006).

[26] K. Krynicki, C. D. Green, and D. W. Sawyer, Far. Disc. Chem. Soc. **66**, 199 (1978).

[27] P. A. Netz, F. W. Starr, H. E. Stanley, and M. C. Barbosa, J. Chem. Phys. **115**, 344 (2001).

[28] F. W. Starr, F. Sciortino, and H. E. Stanley, Phys. Rev. E **60**, 6757 (1999).

[29] A. Demurov, R. Radhakrishnan, and B. L. Trout, J. Chem. Phys. **116**, 702 (2002).

[30] K. Goto, T. Hondoh, and A. Higashi, Jpn. J. Appl. Phys. **25**, 351 (1986).

[31] A. Kalra, S. Garde, and G. Hummer, PNAS **100**, 10175 (2003).

[32] J. Marty, G. Nagy, M. C. Gordillo, and E. Guàrdia, J. Chem. Phys. **124**, 094703 (2006).

[33] A. Pertsin, and M. Grunze, J. Phys. Chem. B **108**, 1357 (2004).

[34] Y. Leng, and P. T. Cummings, Phys. Rev. Lett. **94**, 026101 (2005).

[35] S. Vaitheeswaran, H. Yin, and J. C. Rasaiah, J. Phys. Chem. B **109**, 6629 (2005).

[36] K. Koga, and H. Tanaka, J. Chem. Phys. **122**, 104711 (2005).

[37] S. H. Lee, and P. J. Rossky, J. Chem. Phys. **100**, 3334 (1994).

[38] F. H. Stillinger, and A. Rahman, J. Chem. Phys. **60**, 1545 (1974).

[39] S. Pal, S. Balasubramanian, and B. Bagchi, Phys. Rev. E **67**, 061502 (2003).

[40] C. S. Lin, R. Q. Zhang, S. T. Lee, M. Elstner, T. Frauenheim, and L. J. Wan, J. Phys. Chem. B **109**, 14183 (2005).

[41] D. Feller, J. Phys. Chem. A **103**, 7558 (1999).

[42] S. Xu, S. Irle, D. G. Musaev, and M. C. Lin, J. Phys. Chem. A **109**, 9563 (2005).

[43] S. Tsuzuki, K. Honda, T. Uchimaru, M. Mikami, and K. Tanabe, J. Am. Chem. Soc. **124**, 104 (2002).

[44] G. D. Smith, and R. L. Jaffe, J. Phys. Chem. **100**, 9624 (1996).

[45] M. O. Sinnokrot, E. F. Valeev, and C. D. Sherrill, J. Am. Chem. Soc. **124**, 10887 (2002).

VITA

Name: Pussana Hirunsit

Address: Department of Chemical Engineering, Dwight Look College of Engineering-Texas A&M University
200 Jack E. Brown Building
3122 TAMU, College Station, Texas 77843-3122

Email Address: pussana.hirunsit@chemail.tamu.edu

Education: B.Eng., Chemical Engineering, King Mongkut's Institute of Technology Ladkrabang, Bangkok, Thailand, 2000
M.Eng., Chemical Engineering, King Mongkut's University of Technology Thonburi, Bangkok, Thailand, 2002
M.S., Chemical Engineering, Texas A&M University, 2007

Scholarship: 2000-2002 Full support from Chemical Engineering Practice School, King Mongkut's University of Technology Thonburi, Bangkok, Thailand
2005-2007 Full support from National Nanotechnology Center, Bangkok, Thailand

Publications: P. Hirunsit, Z. Huang, T. Srinophakun, M. Charoenchaitrakool, S. Kaw, *Particle formation of ibuprofen–supercritical CO2 system from rapid expansion of supercritical solutions (RESS): A mathematical model.* Powder Technology, 2005. **154**: p. 83-94.
P. Hirunsit and P. B. Balbuena, *"The effects of confinement on water structure and dynamics: A molecular simulation study,"* J. Phys. Chem. C, 2007. **111**: p. 1709-1715.